Atmos. Chem. Phys., 17, 6611–6629, 2017
https://doi.org/10.5194/acp-17-6611-2017

Atmospheric Chemistry and Physics
Open Access
EGU

Influence of urban pollution on the production of organic particulate matter from isoprene epoxydiols in central Amazonia

Suzane S. de Sá[1], Brett B. Palm[2], Pedro Campuzano-Jost[2], Douglas A. Day[2], Matthew K. Newburn[3], Weiwei Hu[2], Gabriel Isaacman-VanWertz[4,a], Lindsay D. Yee[4], Ryan Thalman[5], Joel Brito[6,b], Samara Carbone[6], Paulo Artaxo[6], Allen H. Goldstein[4], Antonio O. Manzi[7], Rodrigo A. F. Souza[8], Fan Mei[9], John E. Shilling[3,9], Stephen R. Springston[5], Jian Wang[5], Jason D. Surratt[10], M. Lizabeth Alexander[3], Jose L. Jimenez[2], and Scot T. Martin[1,11]

[1]School of Engineering and Applied Sciences, Harvard University, Cambridge, Massachusetts, USA
[2]Department. of Chemistry & Biochemistry and Cooperative Institute for Research in Environmental Sciences, University of Colorado, Boulder, Colorado, USA
[3]Environmental Molecular Sciences Laboratory, Pacific Northwest National Laboratory, Richland, Washington, USA
[4]Dept. of Environmental Science, Policy, and Management, University of California, Berkeley, California, USA
[5]Brookhaven National Laboratory, Upton, New York, USA
[6]Departamento de Física Aplicada, Universidade de São Paulo, São Paulo, Brazil
[7]Instituto Nacional de Pesquisas da Amazonia, Manaus, Amazonas, Brazil
[8]Escola Superior de Tecnologia, Universidade do Estado do Amazonas, Manaus, Amazonas, Brazil
[9]Atmospheric Sciences and Global Change Division, Pacific Northwest National Laboratory, Richland, WA, USA
[10]Department of Environmental Sciences and Engineering, Gillings School of Global Public Health, The University of North Carolina at Chapel Hill, Chapel Hill, North Carolina, USA
[11]Department of Earth and Planetary Sciences, Harvard University, Cambridge, Massachusetts, USA
[a]now at: Massachusetts Institute of Technology, Cambridge, Massachusetts, USA
[b]now at: Laboratory for Meteorological Physics (LaMP), University Blaise Pascal, Aubière, France

Correspondence to: Scot T. Martin (scot_martin@harvard.edu)

Received: 16 November 2016 – Discussion started: 13 December 2016
Revised: 26 April 2017 – Accepted: 28 April 2017 – Published: 6 June 2017

Abstract. The atmospheric chemistry of isoprene contributes to the production of a substantial mass fraction of the particulate matter (PM) over tropical forests. Isoprene epoxydiols (IEPOX) produced in the gas phase by the oxidation of isoprene under HO_2-dominant conditions are subsequently taken up by particles, thereby leading to production of secondary organic PM. The present study investigates possible perturbations to this pathway by urban pollution. The measurement site in central Amazonia was located 4 to 6 h downwind of Manaus, Brazil. Measurements took place from February through March 2014 of the wet season, as part of the GoAmazon2014/5 experiment. Mass spectra of organic PM collected with an Aerodyne Aerosol Mass Spectrometer were analyzed by positive-matrix factorization. One resolved statistical factor ("IEPOX-SOA factor") was associated with PM production by the IEPOX pathway. The IEPOX-SOA factor loadings correlated with independently measured mass concentrations of tracers of IEPOX-derived PM, namely C_5-alkene triols and 2-methyltetrols ($R = 0.96$ and 0.78, respectively). The factor loading, as well as the ratio f of the loading to organic PM mass concentration, decreased under polluted compared to background conditions. For an increase in NO_y concentration from 0.5 to 2 ppb, the factor loading and f decreased by two to three fold. Overall, sulfate concentration explained 37 % of the variability in the factor loading. After segregation of factor loading into subsets based on NO_y concentration, the sulfate concentration explained up to 75 % of the variability. Considering both factors, the data sets show that the suppressing effects of increased NO concentrations dominated over the enhancing effects of higher sulfate concentrations. The pollution from Manaus elevated NO_y concentrations more significantly than sulfate concen-

trations relative to background conditions. In this light, increased emissions of nitrogen oxides, as anticipated for some scenarios of Amazonian economic development, could significantly alter pathways of PM production that presently prevail over the tropical forest, implying changes to air quality and regional climate.

1 Introduction

Organic compounds comprise up to 90 % of the mass concentration of submicron organic particulate matter (PM) over tropical forests (Kanakidou et al., 2005). Submicron PM has adverse effects on human health (Nel, 2005; Pope III and Dockery, 2006) and influences air quality and climate by scattering radiation and acting as cloud condensation nuclei (Ramanathan et al., 2001; Kaufman et al., 2002). A significant fraction of the submicron organic material originates from secondary processes, mainly by the atmospheric oxidation of volatile organic compounds (VOCs) emitted as part of natural and human activities (Zhang et al., 2007; Hallquist et al., 2009; Jimenez et al., 2009). The particle life cycle over Amazonia is in particular strongly influenced by secondary processes that produce organic PM (Martin et al., 2010a; Pöschl et al., 2010). Biogenic emissions from tropical forests are high, and environmental conditions favor photooxidation reactions. The reactive chemistry and the relative importance of pathways leading to PM production can be strongly guided by regulating species, such as sulfate and nitric oxide (NO) (Surratt et al., 2007a; Worton et al., 2013; Liu et al., 2016a). The concentrations of these species depend on their background occurrence, pollution sources, and the relative mix of background and polluted air masses.

Over tropical forests such as Amazonia, the atmospheric chemistry of isoprene produces a substantial fraction of the submicron organic PM (Chen et al., 2009, 2015; Robinson et al., 2011; Isaacman-VanWertz et al., 2016). Isoprene (2-methyl-1,3-butadiene, C_5H_8) is the non-methane VOC most abundantly emitted by tropical forests (Guenther et al., 2012), and isoprene epoxydiols (IEPOX) have been identified as important intermediates in the production of PM from isoprene (Paulot et al., 2009; Surratt et al., 2010; Lin et al., 2012). A chemical sequence for the production of IEPOX-derived PM from the photooxidation of isoprene in the atmosphere is represented in Fig. 1. The sequence is initiated when isoprene peroxy radicals (ISOPOO) are produced in the gas phase by reactions between isoprene and photochemically generated hydroxyl radicals (OH). The reactive fate of the ISOPOO radicals can differ under background compared to polluted conditions (Surratt et al., 2010; Crounse et al., 2011; Worton et al., 2013).

Under background conditions, meaning that HO_2 pathways are favorable in the absence of extensive NO pollution (Wennberg, 2013; Liu et al., 2016a), the ISOPOO radicals continue in large part through the series of species highlighted in yellow in Fig. 1. Through HO_x-facilitated reaction steps, the ISOPOO radicals produce hydroperoxides (ISOPOOH) as major first-generation products and subsequently IEPOX as major second-generation products (Carlton et al., 2009; Paulot et al., 2009; Liu et al., 2013, 2016a; St. Clair et al., 2015). Some of the produced IEPOX undergoes reactive uptake to particles, as facilitated by hydronium ions at the surface (Surratt et al., 2007a; Lin et al., 2012; Gaston et al., 2014; Kuwata et al., 2015; Lewandowski et al., 2015). This chemical sequence can contribute a significant fraction of submicron PM mass concentration over tropical forests (Claeys et al., 2004; Hu et al., 2015). Laboratory studies indicate that about half of the PM produced by isoprene photooxidation under HO_2-dominant conditions in the presence of acidic sulfate particles is associated with IEPOX production and uptake (Liu et al., 2015). Interaction of IEPOX with cloud waters warrants investigation (Lim et al., 2005; Ervens et al., 2011; Budisulistiorini et al., 2015; Chen et al., 2015). In addition to IEPOX pathways, laboratory studies suggest that multifunctional hydroperoxides produced in the gas phase can contribute to isoprene-derived PM production (Krechmer et al., 2015; Liu et al., 2016b; Riva et al., 2016b).

After reactive uptake of IEPOX, particle-phase reactions can produce several different families of species. These species are collectively labeled "IEPOX-derived PM" and represent a subset of the ambient organic PM, as labeled in Fig. 1. The presence of 2-methyltetrols, C_5-alkene triols, 3-methyltetrahydrofuran-3,4-diols, organosulfates, and related oligomers in ambient PM is an indicator of PM production by IEPOX uptake under atmospheric conditions (Claeys et al., 2004; Surratt et al., 2006, 2007b, 2010; Robinson et al., 2011; Lin et al., 2012, 2014). Even though these species may differ in some cases from the actual compounds in the atmospheric PM due to thermal decomposition during analysis (Lopez-Hilfiker et al., 2016), they serve as chemical tracers for the atmospheric concentration of IEPOX-derived PM (Hu et al., 2015; Isaacman-VanWertz et al., 2016). The analytical methods highlighted in Fig. 1, including that of retrieving an "IEPOX-SOA factor" from mass spectral analysis used herein, can lead to over- and underestimated IEPOX-derived PM concentrations. This uncertainty is represented in the figure by the brown dashed lines that approximately but not exactly correspond to IEPOX-derived PM.

Under polluted conditions, the reactive sequence of isoprene and ultimately PM production can become significantly altered (Fig. 1). NO concentrations can be sufficiently high that ISOPOO radicals react almost entirely with NO in place of HO_2, thereby largely producing methacrolein (MACR) and methyl vinyl ketone (MVK) in place of ISOPOOH (Liu et al., 2016a). As a result, IEPOX production can be greatly decreased, ultimately reducing PM production by IEPOX pathways. A minor channel along the NO pathway can still produce IEPOX, although much less efficiently (Jacobs et al., 2014). Under NO-dominant conditions,

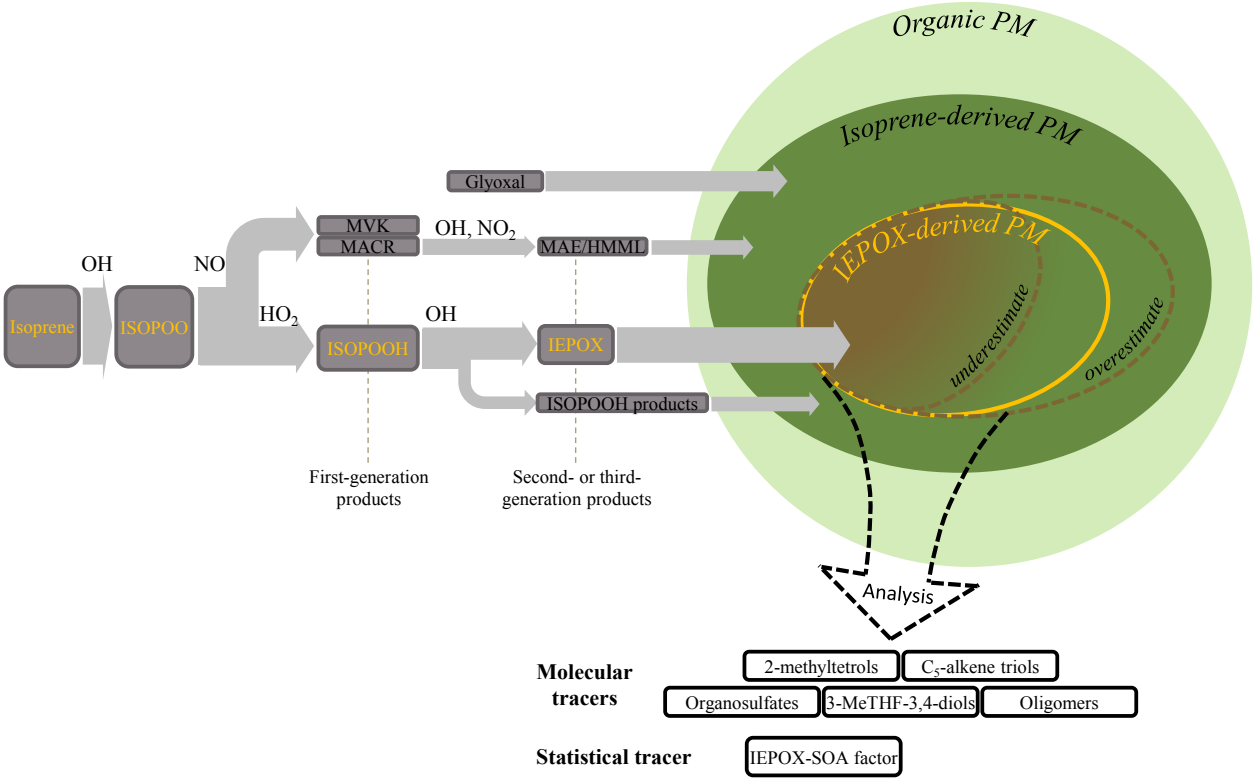

Figure 1. Schematic diagram for the production of PM derived from isoprene epoxydiols (IEPOX) produced during the photooxidation of isoprene. Organic peroxy radicals (ISOPOO), produced by OH attack and O_2 addition to isoprene, are scavenged along NO or HO_2 pathways. By the HO_2 pathway, organic hydroperoxides (ISOPOOH) are first-generation products that react with additional OH to produce IEPOX. The IEPOX species undergo reactive uptake into particles, ultimately producing IEPOX-derived particulate matter. Arrow thickness qualitatively illustrates the relative importance (i.e., mass flux) of a reaction channel under background conditions. Gray and green background colors indicate species in the gas and particle phases, respectively. The light-green disk represents the total organic PM. Within that disk, the contribution by isoprene-derived PM, including compounds produced both IEPOX and non-IEPOX pathways, is represented by the dark-green oval. Inside that oval, the contribution by IEPOX-derived PM is represented by the yellow oval region. The color gradient between brown and dark green illustrates the chemical modification of the IEPOX-derived PM over time. The large dashed black arrow represents the analytical methods that use different types of molecular and statistical tracers (listed in the boxes) to quantify the IEPOX-derived PM mass concentrations. For simplicity, the figure omits the many routes leading to the production of glyoxal (Fu et al., 2008), possible ISOPOO isomerization when NO and HO_2 concentrations are sufficiently low (Crounse et al., 2011; Liu et al., 2016a), second-generation production of peroxymethacrylic nitric anhydride (Lin et al., 2013; Nguyen et al., 2015), and particle water and other inorganic components. 3-methyltetrahydrofuran-3,4-diols are abbreviated as 3-MeTHF-3,4-diols. Other abbreviations are provided in the main text.

alternative pathways of PM production not involving IEPOX can become active, though in lower yields. MACR can be oxidized to produce peroxymethacrylic nitric anhydride (MPAN), which is a precursor to methacrylic acid epoxide (MAE) and hydroxymethylmethyl-α-lactone (HMML), and these compounds can undergo reactive uptake to produce PM (Kjaergaard et al., 2012; Lin et al., 2013; Worton et al., 2013; Nguyen et al., 2015). Glyoxal produced from isoprene oxidation can contribute to PM production (Volkamer et al., 2007; Ervens and Volkamer, 2010; McNeill et al., 2012; Marais et al., 2016).

Another possible mechanism affecting PM production by IEPOX uptake under polluted conditions is altered particle composition, especially particle acidity, largely driven by sulfate. Laboratory studies show that IEPOX uptake increases with increasing acidity (Gaston et al., 2014; Kuwata et al., 2015; Liu et al., 2015). A proposed reaction during uptake is the acid-catalyzed ring opening of the IEPOX molecule (Surratt et al., 2010). The subsequent particle-phase reactions include the addition of available nucleophiles, such as water to produce tetrols or sulfate to produce organosulfates as well as their oligomers (Surratt et al., 2010; Lin et al., 2014; Nguyen et al., 2014). In support of this proposed mechanism, analyses by positive-matrix factorization (PMF) of mass spectra collected in the southeastern USA identified PMF factors associated with IEPOX-derived PM, and these factors correlated positively with sulfate mass concentrations (Budisulistiorini et al., 2013; Hu et al., 2015;

Xu et al., 2015). In short, different regimes of $NO : HO_2$ concentration ratios and different possible PM compositions between polluted and background conditions can lead to different product distributions and different production rates of IEPOX-derived PM.

The extent to which pollution may shift the production pathways of IEPOX-derived PM over tropical forests remains to be elucidated. The study described herein is based on data sets collected in the wet season downwind of Manaus, Brazil, during the Observations and Modeling of the Green Ocean Amazon (GoAmazon2014/5) experiment (Martin et al., 2016a). The research site was influenced at times and to variable extents by the pollution outflow from the Manaus metropolitan area. Compared to the background environment in Amazonia, the Manaus plume had high number concentrations of particles and enhanced concentrations of pollutants, including oxides of nitrogen and sulfate (Kuhn et al., 2010; Martin et al., 2016a). The reactive gas-phase chemistry was strongly guided by the relative mix of background and polluted air masses (Trebs et al., 2012; Liu et al., 2016a). The analysis herein focuses on how the pollution perturbed IEPOX-derived PM production relative to background conditions.

2 Methodology

Data sets were collected at the "T3" site (3.2133° S, 60.5987° W) located 70 km to the west of Manaus, Brazil, in central Amazonia (Martin et al., 2016a). The site was situated in a pasture (2.5 km × 2 km) surrounded by forest. The analysis herein focuses on data sets collected during the wet season period of 1 February to 31 March 2014, corresponding to the first Intensive Operating Period (IOP1) of the GoAmazon2014/5 experiment.

A High-Resolution Time-of-Flight Aerosol Mass Spectrometer (HR-ToF-AMS, hereafter AMS; Aerodyne, Inc., Billerica, Massachusetts, USA) recorded the primary data set of this study. The AMS provided quantitative bulk characterization of the atmospheric PM. The design principles and capabilities of this instrument are described in the literature (DeCarlo et al., 2006; Canagaratna et al., 2007). The instrument was housed within a temperature-controlled research container, and the inlet to the instrument sampled from 5 m above ground level. Detailed aspects of AMS operation are presented in the Supplement (Sect. S1). In brief, ambient measurements were obtained every other 4 min. Organic, sulfate, ammonium, nitrate, and chloride PM mass concentrations were obtained from "V-mode" data. The choice of ions to fit was aided by the "W-mode" data, which were collected for 1 day every 5 days. Data analysis was performed using SQUIRREL (1.56D) and PIKA (1.14G) of the AMS software suite.

Positive-matrix factorization was applied to the time series of the organic component of the high-resolution mass spectra (Ulbrich et al., 2009). The present study focuses on one of the resolved statistical factors, referred to as the IEPOX-SOA factor (Hu et al., 2015). Diagnostics of the PMF analysis, especially as related to the resolved IEPOX-SOA factor, are presented in the Supplement (Sect. S2). A separate account is forthcoming to present the other PMF factors (de Sá, 2017). Herein, "factor profile" and "factor loading" refer to the mathematical products of the multivariate statistical analysis, whereas "mass spectrum" and "mass concentration" refer to measurements.

Complementary to the AMS data sets, mass concentrations of molecular and tracer organic species were measured using a semivolatile thermal desorption aerosol gas chromatograph (SV-TAG) at a time resolution of 1 h. The instrument collected gas and particle samples, followed by thermal desorption, derivatization, and gas chromatography coupled to mass spectrometry (Isaacman et al., 2014). A summary of operational details for GoAmazon2014/5 is presented in the Supplement (Sect. S1), and the main account is presented in Isaacman-VanWertz et al. (2016).

Additional data sets used in the analysis were collected at the T3 site by instruments housed in the research container of the Mobile Aerosol Observing System (MAOS) of the ARM Climate Research Facility (ACRF) operated by the USA Department of Energy (Mather and Voyles, 2013; Martin et al., 2016a). A temperature-controlled inlet was mounted at 10 m above ground level. Measurements of nitrogen oxides were made using a chemiluminescence-based instrument (Air Quality Design). The measured odd-nitrogen family "NO_y", meaning NO_x plus reservoir species, included NO, NO_2, HNO_3, organonitrates, particle nitrate, and peroxyacetyl nitrates. Further details of the NO_y measurements are presented in the Supplement (Sect. S1). Ozone concentrations were measured by an ozone analyzer (Thermo Fisher, model 49i). Particle number concentrations were measured by a condensation particle counter (TSI, model 3772). Meteorological variables provided by the ARM Mobile Facility (AMF-1), which was also part of the ACRF, included wind direction, solar irradiance, and precipitation rate. Measurements of NO_y and particle number concentration onboard the G-1 aircraft of the ARM Aerial Facility (AAF) were also used in the analysis (Schmid et al., 2014; Martin et al., 2016a).

3 Results and discussion

The organization of the presentation herein is as follows. The factor profile obtained from AMS PMF analysis is discussed (Sect. 3.1), a case study comparing factor loading under background to polluted conditions is presented (Sect. 3.2), the roles of sulfate (Sect. 3.3) and nitric oxide (Sect. 3.4) in affecting factor loading are explored, and the influence of

NO on production and loss processes of IEPOX-derived PM is considered (Sect. 3.5).

3.1 Statistical IEPOX-SOA factor

Positive-matrix factorization was carried out on the time series of AMS organic mass spectra. One statistical factor had a similar profile of peak intensities as the IEPOX-SOA factor identified in other studies (Fig. S1 in the Supplement) (Robinson et al., 2011; Slowik et al., 2011; Budisulistiorini et al., 2013, 2015; Chen et al., 2015; Xu et al., 2015). The Pearson correlation coefficient R between this factor and the one obtained in the 2008 wet season in central Amazonia as part of the AMAZE-08 experiment was 0.99 (Chen et al., 2015). The ratio f of the factor loading to the mass concentration of submicron organic PM for the present study was 0.17 ± 0.09 (mean $\pm$ standard deviation). The IEPOX-SOA factor has been identified previously over the maritime tropical forest of Borneo ($f = 0.23$) (Robinson et al., 2011), in a rural area in Canada 70 km north of Toronto ($f = 0.17$) (Slowik et al., 2011), across several locations in the southeastern USA in summertime ($f = 0.17$ to 0.41) (Budisulistiorini et al., 2013, 2015, 2016; Hu et al., 2015; Xu et al., 2015; Marais et al., 2016), and in AMAZE-08 ($f = 0.34$) (Chen et al., 2015). A further review of the ubiquity and characteristics of the IEPOX-SOA factor is presented in Hu et al. (2015).

The IEPOX-SOA factor reported herein had prominent peaks at m/z 53.04 and m/z 82.04 (Fig. S1). The ion at m/z 82.04, corresponding to $C_5H_6O^+$, has been attributed to 3-methylfuran (3-MF). The thermal degradation of isoprene-derived PM upon mass spectral analysis was suggested as the source of 3-MF (Robinson et al., 2011). Lin et al. (2012) proposed that sequential dehydrations upon mass spectral analysis of 3-methyltetrahydrofuran-3,4-diols, which are an identified component of IEPOX-derived PM, can produce 3-MF. Other IEPOX-derived species as well as non-IEPOX species might also contribute to the production of $C_5H_6O^+$ ions (Surratt et al., 2010; Hu et al., 2015; Liu et al., 2016c).

Laboratory studies show that a mass spectrum that is a pattern of peak intensities similar to that of the IEPOX-SOA factor is produced by the uptake of IEPOX into aqueous acidic sulfate particles as well as by the photooxidation of isoprene under HO_2-dominant conditions in the presence of acidic sulfate particles (Budisulistiorini et al., 2013; Nguyen et al., 2014; Kuwata et al., 2015; Liu et al., 2015). The possibility of similar uptake by a broader range of liquid media remains to be fully tested, such as other acidic solutions as well as cloud waters. Compared to the laboratory spectra of Liu et al. (2015), representing about 4 h of OH exposure at atmospheric concentrations (1.7×10^6 molec cm^{-3}), the main difference was the relative intensity of the m/z 44 peak. For the IEPOX-SOA factor of the present study, this peak was 4 times more intense (Fig. S1), suggesting that the atmospheric PM was more oxidized. Hu et al. (2016) showed that heterogeneous aging of IEPOX-SOA can result in increased relative signal at m/z 44.

By contrast, laboratory studies show that a significantly different mass spectrum from that of the IEPOX-SOA factor is obtained for PM produced from isoprene photooxidation in the absence of aqueous particles (Krechmer et al., 2015; Kuwata et al., 2015). Under these conditions, chemical pathways other than IEPOX uptake into a liquid medium appear to be active, such as the condensation of low-volatility, multifunctional compounds produced by additional oxidation of ISOPOOH (Krechmer et al., 2015; Liu et al., 2016b; Riva et al., 2016b). This non-IEPOX pathway, however, is not expected to contribute a large fraction of the produced PM during the study period because of the high relative humidity conditions in Amazonia and the prevalence of liquid particles for the prevailing atmospheric conditions (Bateman et al., 2016; de Sá, 2017).

The SV-TAG measurements of the concentrations of C_5-alkene triols and 2-methyltetrols support the interpretation of the IEPOX-SOA factor as an indicator that PM was being produced, at least in significant part, from the reactive uptake of IEPOX (Claeys et al., 2004; Wang et al., 2005; Surratt et al., 2010). The factor loading strongly correlated with the concentrations of C_5-alkene triols ($R = 0.96$) and 2-methyltetrols ($R = 0.78$) (Fig. 2). These species have been associated with the IEPOX reaction pathway in several laboratory studies (Surratt et al., 2010; Riedel et al., 2016). The R value with respect to C_5-alkene triols was independent of the f_{peak} value of the PMF solution, demonstrating the robustness of the relative time trend of factor loading even though the factor profile and absolute loadings changed across f_{peak} values (Fig. S2d).

The loading of the IEPOX-SOA factor may be an overestimate or an underestimate of the atmospheric concentration of the IEPOX-derived PM (Supplement, Sect. S2). The IEPOX-SOA factor can be understood as the net result of (i) produced IEPOX-derived PM, (ii) minus that portion of the carbon that gets further oxidized and mixed into other PMF factors, and (iii) plus that portion of non-IEPOX-derived PM that gives rise to a similar AMS mass spectral pattern as the IEPOX-derived PM (Supplement, Sect. S2). Processes of type ii contribute to underestimates and processes of type iii lead to overestimates when using IEPOX-SOA factor loading as a surrogate for IEPOX-derived PM concentration. These uncertainties are qualitatively represented in Fig. 1 by the brown dashed lines that enclose the fraction of particle material statistically captured by the factor analysis. The further analysis herein is based on using the loading of the IEPOX-SOA factor as a scalar proxy for the mass concentration of IEPOX-derived PM in a sampled air mass.

3.2 Background compared to polluted conditions

Under background conditions in the wet season, remote areas of the Amazon forest constitute one of the least-polluted

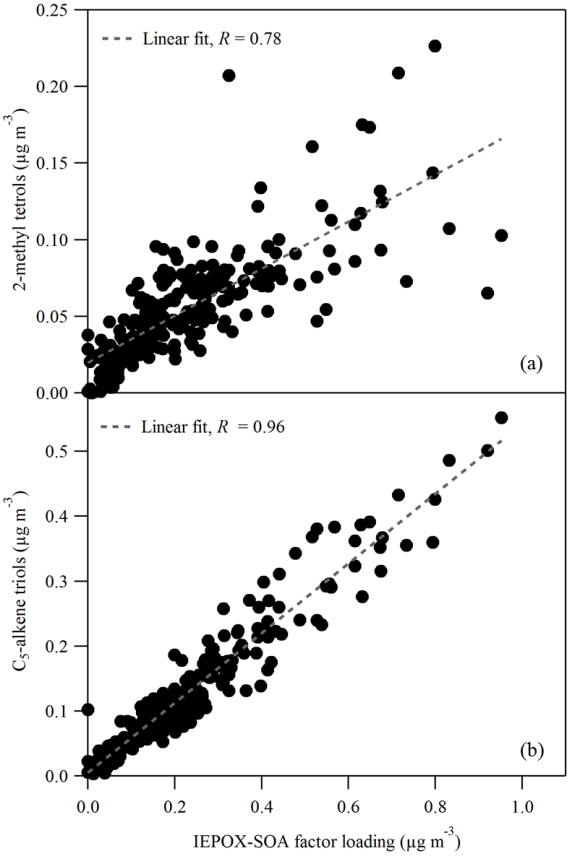

Figure 2. Scatter plot of the loading of the IEPOX-SOA factor derived from analysis of the AMS data set and the mass concentrations of C_5-alkene triols and 2-methyltetrols measured by SV-TAG. All data collected during the IOP1 period are included, meaning that the plotted data are not limited to afternoon time periods.

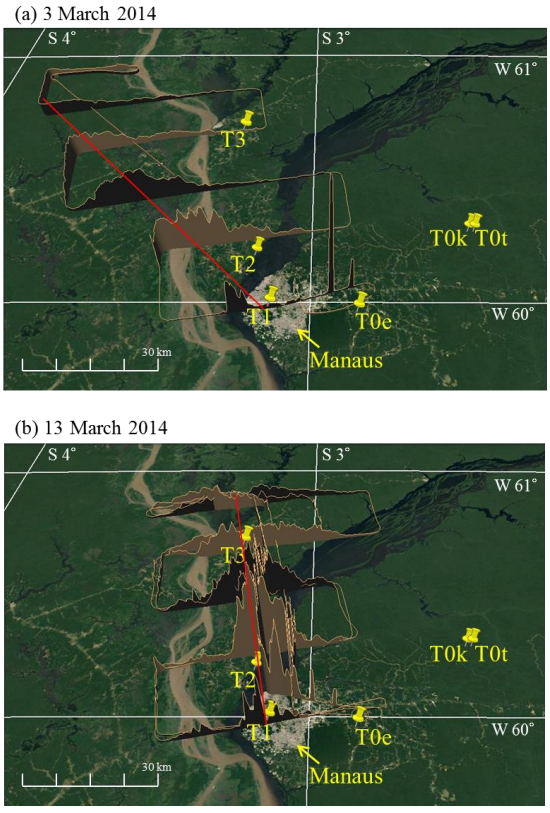

Figure 3. Visualization of the Manaus pollution plume by plotting particle number concentrations in the vertical axis. Observations took place on flights from late morning to early afternoon on **(a)** 3 March 2014, 17:45–19:26 UTC, and **(b)** 13 March 2014, 14:14–17:21 UTC. Local time is UTC − 4 h. The red lines guide the eye through the central axis of the plume. The direction and extent of the plume was observed by the G-1 aircraft within the atmospheric boundary layer downwind of Manaus. Measured particle number concentrations are plotted on a vertical axis on top of an image of land cover in the horizontal plane. Particle concentrations in the center of the plume ranged from 10 000 to 25 000 cm^{-3} nearby Manaus. Yellow pins indicate the locations of some of the GoAmazon2014/5 research sites, including T3 (Martin et al., 2016a).

continental regions on Earth (Martin et al., 2010a). Nitric oxide concentrations characteristic of central Amazonia range from 20 to 70 ppt (Torres and Buchan, 1988; Bakwin et al., 1990; Levine et al., 2015). Daytime maximum ozone concentrations are 10 to 15 ppb (Rummel et al., 2007). Sulfate mass concentrations associated with in-basin processes are on average $< 0.1\,\mu g\,m^{-3}$, and total background sulfate concentrations contributed by in- and out-of-basin processes rarely exceed $0.5\,\mu g\,m^{-3}$ (Andreae et al., 1990; Chen et al., 2009).

In the wet season, Manaus emissions were the most important anthropogenic influence on observations at the T3 research site (Martin et al., 2017). The afternoons of 3 and 13 March 2014 are presented herein as representative cases of background and polluted conditions, respectively. Both days were sunny, and major precipitation events were absent. Particle number concentrations measured onboard the G-1 aircraft within the atmospheric boundary layer show the position of the pollution plume on these two afternoons (Fig. 3). NO_y concentrations measured during the same flight are shown in Fig. S3. The visualization in Fig. 3 shows that on 3 March the Manaus plume passed south of the T3 site. By comparison, on 13 March the central portion of the plume passed over T3. Aircraft-based observations to track the Manaus plume were available for 16 afternoons of the 2-month study period.

Measurements at ground level at the T3 site are plotted in Fig. 4 for the afternoons of 3 March (left panel) and 13 March (right panel). Based on wind speeds, the research site was 4 to 6 h downwind of Manaus (Martin et al., 2016a). Anthropogenic-biogenic interactions affecting the production of IEPOX-derived PM were driven in large part by atmospheric photochemistry at daybreak. Morning urban emissions followed by atmospheric processing arrived at the T3 site during the local afternoon. The afternoon period, in ad-

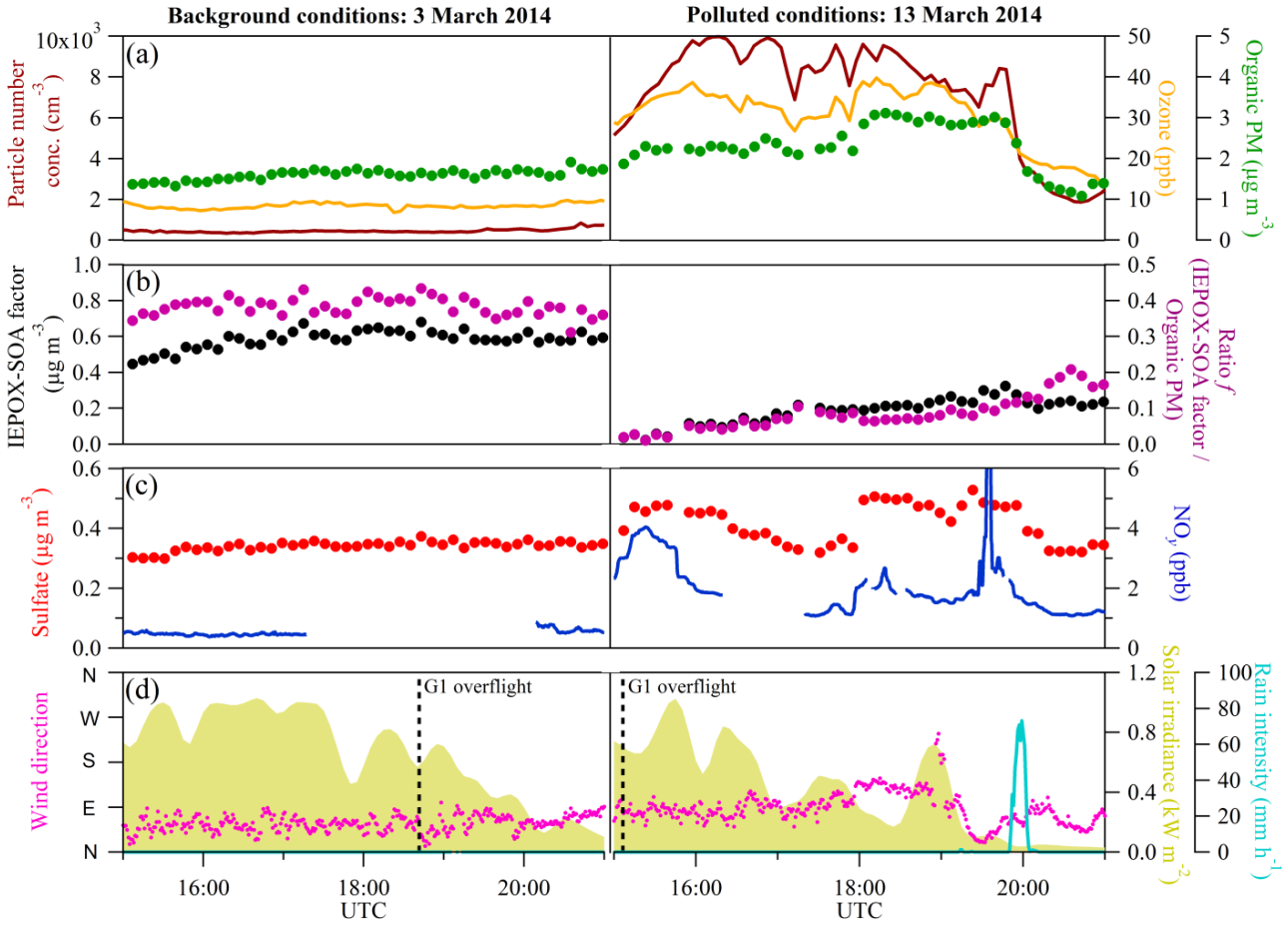

Figure 4. Case studies of (left) background and (right) polluted air masses passing over T3 on afternoons of 3 and 13 March 2014. **(a)** Ozone, particle number, and organic mass concentration. **(b)** IEPOX-SOA factor loading and the ratio f of the factor loading to the organic PM concentration. **(c)** Sulfate and NO_y concentrations. **(d)** Wind direction, rain intensity, and solar irradiance. Local time is UTC − 4 h. Time points of overflights at 500 m by the G-1 research aircraft are marked by the dashed line (Martin et al., 2016a).

dition to the connection to the Manaus plume, was also characterized by reduced variability in other possible confounding variables, such as temperature, radiation, and relative humidity. Figure 4 shows that on the afternoon of 3 March ozone concentrations were below 10 ppb, particle number concentrations were below 1000 cm^{-3}, NO_y concentrations were less than 1 ppb, and sulfate concentrations were 0.3 to 0.4 μg m^{-3}. Species concentrations were stable throughout the afternoon. On 13 March, ozone concentrations exceeded 30 ppb for most of the afternoon, particle concentrations reached 10 000 cm^{-3}, NO_y concentrations consistently exceeded 1 ppb, and sulfate concentrations were 0.3 to 0.6 μg m^{-3}. Concentrations fluctuated markedly throughout the afternoon on 13 March, reflecting different levels of pollution influence in the air passing over the T3 site during that period.

Elevated concentrations of ozone, particle number, and NO_y were reliable markers of pollution influence over the course of the study period (Supplement, Sect. S3). Pollution was associated with stronger relative enhancements in NO_y concentrations than in sulfate concentrations (Sect. 3.3 and 3.4). With respect to the IEPOX-SOA factor, Fig. 4 shows that the absolute and relative loadings decreased for the polluted compared to background conditions. Relative loadings are expressed by the ratio f of IEPOX-SOA factor loading to the organic PM mass concentration. Decreased absolute and relative factor loadings under polluted conditions, presented in Fig. 4 as a case study, also characterized the data sets of the entire study period. Other examples are presented in the Supplement (Fig. S4).

3.3 Sulfate as a driver of IEPOX-derived PM production

A scatter plot between sulfate mass concentrations and IEPOX-SOA factor loadings for all afternoon periods is shown in Fig. 5a. Background and polluted conditions are represented in the data set. For further visualization, the data

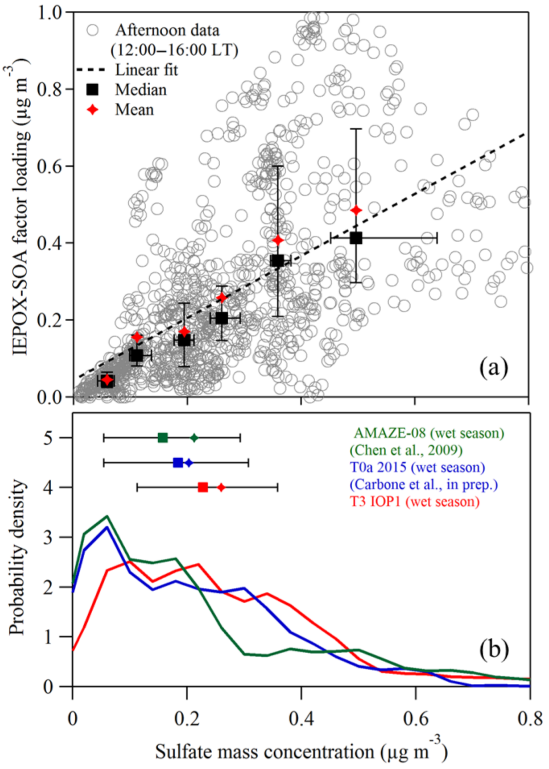

Figure 5. (a) Scatter plot of sulfate mass concentration and IEPOX-SOA factor loading. A least-squares linear fit is represented by the dashed line ($R^2 = 0.37$). The data set was collected into six subsets based on sulfate concentration to calculate statistics. Medians (squares) and means (diamonds) of each subset are plotted. Whiskers on the medians represent the interquartile ranges. **(b)** Probability density function of sulfate mass concentration at the background site T0t (TT34) north of Manaus in the wet season of 2008 (Chen et al., 2009; Martin et al., 2010b, 2016b), at the background site T0a (ATTO) northeast of Manaus in the wet season of 2015 (Andreae et al., 2015), and at T3 during the wet season of 2014 (IOP1). The plotted data sets were recorded during local afternoons (12:00–16:00 local time; 16:00–20:00 UTC). Means (diamonds), medians (squares), and interquartile range (whiskers) are shown for the probability density functions.

set was organized into six subsets based on sulfate concentration. The medians and the means of the subsets are plotted in the figure. The visualization shows that sulfate concentration served as a first-order predictor of the IEPOX-SOA factor loading in central Amazonia in the wet season. The explanation can be a combination of increased acidity, greater reaction volume including by enhanced hygroscopic growth, and possibly a nucleophilic role for sulfate (Xu et al., 2015; Marais et al., 2016). An analysis of the relative importance of each is out of the scope of the present study (Supplement, Sect. S4).

For Fig. 5a, the coefficient R^2 of determination between sulfate mass concentration and factor loading was 0.37, meaning that 37 % of the variance of the IEPOX-SOA factor loading was explained by sulfate mass concentration. As a point of comparison, R^2 varied between 0.4 and 0.6 for observations in the southeastern USA, which seasonally is a region of high isoprene emissions (Budisulistiorini et al., 2013, 2015; Hu et al., 2015; Xu et al., 2015). A chemical transport model that predicted IEPOX-derived PM mass concentration for the southeastern USA obtained R^2 of 0.4 for the relationship to predicted sulfate mass concentration (Marais et al., 2016). The model attributed the correlation to the acidity and particle volume provided by sulfate, both of which favored IEPOX uptake. Central Amazonia and the southeastern USA differ considerably in terms of meteorology, chemistry, and levels of regional pollution, yet they have in common an important role of sulfate concentration as a predictor of IEPOX-derived PM concentration, even as the sulfate concentrations themselves differ by an order of magnitude. Sulfate concentrations typically had an interquartile range of [1.5, 3.0] $\mu g\,m^{-3}$ in the studies in the southeastern USA, which can be compared to a range of [0.11, 0.36] $\mu g\,m^{-3}$ under background conditions during the wet season in central Amazonia.

A key difference between the southeastern USA and central Amazonia is the role of sulfate concentration as a clear or ambiguous indicator, respectively, of urban influence. For the relatively low sulfate mass concentrations ($< 0.5\,\mu g\,m^{-3}$) characteristic of the study period, background air in central Amazonia contributed significantly to the variability in sulfate concentration measured at the T3 site. Background concentrations of sulfate in Amazonia, distinguished from sulfate tied to the urban Manaus plume, originated from in-basin emissions of gas-phase precursors such as dimethyl sulfide (DMS) and hydrogen sulfide (H_2S) from the forest as well as from out-of-basin marine emissions from the Atlantic Ocean (Andreae et al., 1990; Chen et al., 2009; Martin et al., 2010a). In the wet season, biomass burning from Africa and to a lesser extent from South America also episodically contributed significantly to sulfate concentrations in the Manaus region. In addition, emissions from large cities on the eastern coast of Brazil were important at times when rare meteorological events shifted the northeasterlies typical of the wet season to easterlies (Martin et al., 2017). Manaus contributions to sulfate mass concentrations in an air mass were in addition to these various background sources.

The relative importance of Manaus contributions to the sulfate concentrations in the air masses that passed over T3 was assessed by comparison of the probability density function of sulfate concentration at T3 to those of sites upwind of Manaus (Fig. 5b). The distributions of the two upwind sites had a central tendency of 0.05 to 0.3 $\mu g\,m^{-3}$, suggesting the range of natural concentrations, and a right-side skewness up to 0.6 $\mu g\,m^{-3}$, suggesting the importance of episodic long-range transport (Chen et al., 2009). The figure shows that the distribution at T3 did not differ greatly from those of the upwind sites even though the air masses over T3 regularly transported Manaus pollution. The implication is that Man-

Table 1. Parameters associated with the NO_y groupings of Fig. 6. Listed are the NO_y concentrations and the parameters for least-squares linear fits to each group. R^2 represents the coefficient of determination.

Group	NO_y range (ppb)	Fit slope	Fit intercept	Fit R^2
1	> 0.66	2.16	−0.13	0.75
2	0.66–0.92	1.48	−0.04	0.64
3	0.92–1.55	0.78	0.06	0.24
4	1.55–2.45	0.71	−0.01	0.44
5	> 2.45	0.55	−0.02	0.62

aus sulfate sources, whether primary or secondary, had small contributions relative to background sources when averaged over time. In short, elevated sulfate concentrations on any one afternoon at the T3 site might have arisen because of elevated background concentrations on that day rather than the influence of the Manaus pollution plume. The implications are that (i) sulfate concentration was an ambiguous indicator of urban influence at the T3 site and (ii) increases in sulfate concentrations in pollution events were moderate relative to background concentrations.

3.4 NO as a modulator of IEPOX-derived PM production

In the transport from Manaus to the T3 research site, NO concentration was not conserved, in part because of reactions with ozone and organic peroxy radicals (Martin et al., 2017). In this case, the instantaneous NO concentrations measured at the T3 site did not directly provide information about the fate of ISOPOO radicals along the transport time of 4 to 6 h from Manaus to the T3 site. The collective contributions of NO, NO_2, and their oxidation products were, however, reflected in measurements of NO_y concentrations at the T3 site. The NO_y family is expected to have a longer lifetime than the transport time from Manaus to the T3 site (Romer et al., 2016). The NO_y concentration measured at T3 therefore served as a surrogate for the integrated exposure of the air mass to NO chemistry between Manaus and T3 (Liu et al., 2016a).

Unlike the ambiguity associated with the sulfate concentration, an elevated NO_y concentration served as a clear indicator of anthropogenic influence in an air mass passing over the T3 site. For background conditions over the forest, NO_y originates from NO emitted from soils and other natural sources such as lightning (Bakwin et al., 1990; Jacob and Wofsy, 1990). The probability density function of NO_y concentration under background conditions in the wet season of the central Amazon basin is shown in Fig. 6b (Bakwin et al., 1990). The distribution for measurements at T3 is also shown. Relative to the narrow distribution around 0.5 ppb for background conditions, there is high-side skewness extending up to 4 ppb for the T3 measurements, indicating the clear influence of Manaus emissions on NO_y concentrations.

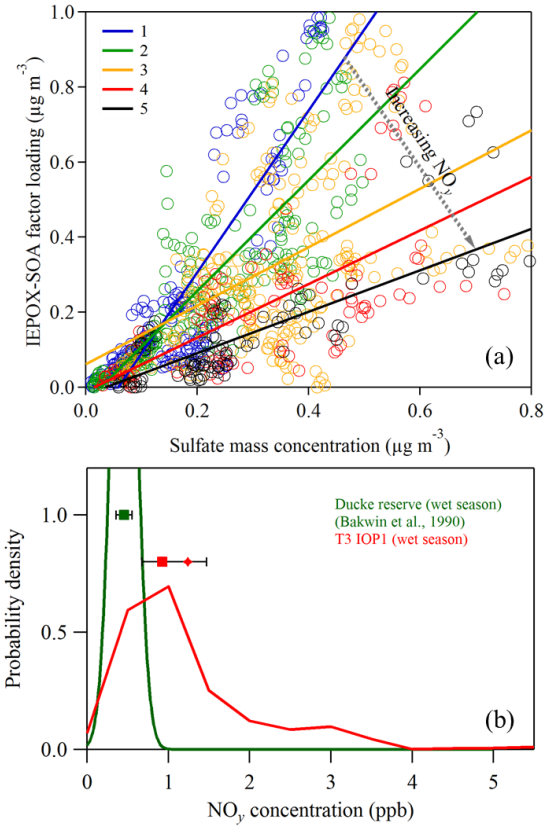

Figure 6. (a) Scatter plot of sulfate mass concentration and IEPOX-SOA factor loading for local afternoon (12:00–16:00 local time; 16:00–20:00 UTC). The data sets were collected into five subsets, colored and labeled 1 to 5, based on NO_y concentration. Table 1 presents the parameters of the five least-squares linear fits represented by the colored lines in the figure. **(b)** Probability density function of NO_y concentration at a background site nearby Manaus in the wet season of 1987 (Bakwin et al., 1990) and at T3 during the wet season of 2014 (IOP1) (afternoon data). Means (diamonds), medians (squares), and interquartile range (whiskers) are shown for the probability density functions. Additional analysis of **(a)** is presented in the Supplement (Sect. S5) related to Fig. S5.

NO_y concentration was incorporated into the analysis by segregation of the data set of Fig. 5a into five subsets (Supplement, Sect. S5). Linear fits to the NO_y-segregated data subsets are plotted in Fig. 6a. Each subset is represented by a different color. Parameter values of the associated fits are listed in Table 1. In conjunction with sulfate concentration, the visualization presented in Fig. 6a shows that NO_y concentration further explained the variability in IEPOX-SOA factor loadings. The R^2 values, representing the extent to which sulfate was able to explain variability in IEPOX-SOA factor loading once isolated for NO_y concentration, were higher for the data subsets with lower and higher extremes of NO_y concentrations (Table 1). These conditions represent

the limiting cases of fully background conditions for the former and the strongest effects of Manaus pollution for the latter. By comparison, intermediate NO_y concentrations could arise from air masses that mixed together background air with Manaus pollution during the transport to T3 (e.g., by entrainment) and thus represent complex processing. Single or multiple mixing points could occur anywhere along the path from Manaus to T3, thus introducing variability into the effective photochemical age of the air mass arriving at T3 and resulting in lower R^2 values for intermediate NO_y concentrations. A caveat is that this explanation assumes that NO emissions from Manaus had low day-to-day variability.

In relation to the influence of Manaus pollution, sulfate concentration was affected by a mixture of background and urban sources (see discussion in Sect. 3.3) whereas NO_y concentration largely had urban sources (see Figs. 5b and 6b). As an approximation to keeping the sulfate concentration constant and thus focusing on the role of NO in the urban pollution, the visualization of the dependence of IEPOX-SOA factor loading on NO_y concentration was further refined by taking data subsets segregated by low ($< 0.1\,\mu g\,m^{-3}$) and high ($> 0.3\,\mu g\,m^{-3}$) sulfate concentrations. Figure 7a, b, and c show the factor loading, organic PM mass concentration, and the ratio f of the IEPOX-SOA factor loading to the organic PM mass concentration, respectively, plotted against NO_y concentration for low and high sulfate concentrations.

Figure 7a shows that for both low and high sulfate concentrations an increase in NO_y concentration from background to polluted concentrations was associated with a decrease in the IEPOX-SOA factor loading by two to three times. For low sulfate concentration, the interquartile range of the factor loading decreased from [0.037, 0.093] to [0.022, 0.039] $\mu g\,m^{-3}$ for an increase in NO_y concentration from 0.5 to 2 pbb. For high sulfate concentration, the factor loading decreased from [0.57, 0.95] to [0.21, 0.35] $\mu g\,m^{-3}$ for the same transition in NO_y concentration. The greatest changes in factor loading were in the region of 1 ppb NO_y. This region of greatest sensitivity coincided with the transition from background to polluted conditions.

For the same time period of these PM analyses of IEPOX-SOA factor loading, Liu et al. (2016a) observed a shift in dominant isoprene gas-phase products from ISOPOOH to MVK/MACR across the transition in NO_y concentration. Liu et al. (2016a) further simulated the dependence on NO concentration of the ratio of the production rate of ISOPOOH to that of MVK + MACR. The highest ratios (0.6 to 0.9) were obtained for background concentrations of NO_y. The calculated HO_2 concentration was $< 4 \times 10^8\,cm^{-3}$ (0.016 ppb). The simulated transition for the dominant fate of the ISOPOO radicals occurred for an NO concentration of < 0.05 ppb.

Figure 7b shows that for both low and high sulfate concentrations the organic PM mass concentration M_{org} and the IEPOX-SOA factor loading had opposite trends for low compared to intermediate NO_y concentrations, even though the

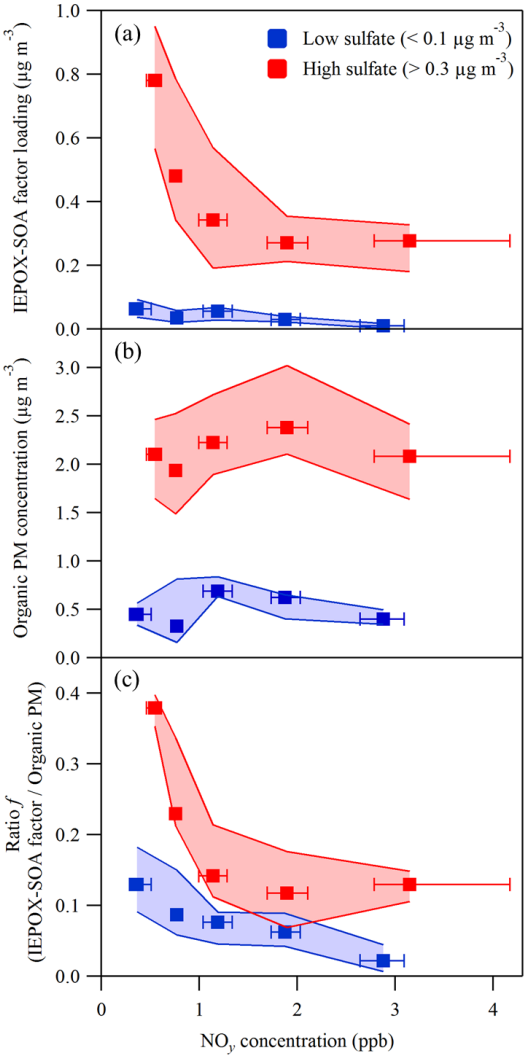

Figure 7. Dependence on NO_y concentration of **(a)** IEPOX-SOA factor loading, **(b)** organic mass concentration, and **(c)** the ratio f of the IEPOX-SOA factor loading to the organic PM concentration. Data are segregated by low ($< 0.1\,\mu g\,m^{-3}$) and high ($> 0.3\,\mu g\,m^{-3}$) sulfate mass concentration and grouped into five levels of NO_y concentration (Fig. 6). Squares represent medians of each group. Interquartile ranges are represented by whiskers along the abscissa and shading along the ordinate. The plotted data sets were recorded during local afternoon (12:00–16:00 local time; 16:00–20:00 UTC).

trend in M_{org} was less steep. The factor loadings decreased by 60 % whereas the M_{org} increased by 25 % for 0.5 to 2 ppb NO_y (Fig. 7a and b). Increases in M_{org} can include contributions from secondary PM produced by enhanced concentrations of hydroxyl radicals and ozone in the pollution plume as well as from primary PM emitted from the Manaus urban region (Martin et al., 2017; de Sá, 2017). For higher NO_y concentrations (> 2 ppb), however, Fig. 7b shows that M_{org} decreased after a peak value, approaching values close to background under the most polluted conditions. The chem-

istry can become sufficiently shifted that more-volatile gas-phase products can be produced (Pandis et al., 1991; Kroll et al., 2005; Carlton et al., 2009). In addition, hydroxyl radical concentrations can also decrease because of titration by NO_2 (Valin et al., 2013; Rohrer et al., 2014). An increase in total organic mass concentration could possibly contribute to a decrease in IEPOX-derived PM production by kinetically limiting the uptake of IEPOX (Gaston et al., 2014; Lin et al., 2014; Riva et al., 2016a). The dominant effect of the urban plume, however, seems to be that of shifting the fate of ISOPOO radicals through the increase in NO, thereby significantly decreasing the production of ISOPOOH (Liu et al., 2016a) (Sect. 3.5).

The combined trends of Fig. 7a and b for increasing NO_y are represented in Fig. 7c as the ratio f. The figure shows that f decreased for increasing NO_y concentration for both low and high sulfate concentrations. The greatest decrease occurred across the range of NO_y concentrations that represented the shift from background to polluted conditions. For low sulfate concentration, the interquartile range of f decreased from [0.09, 0.18] to [0.04, 0.09] for an increase in NO_y concentration from 0.5 to 2 ppb. These ranges shifted to [0.35, 0.40] and [0.07, 0.18] for high sulfate concentration. As a limiting statement, for the most favorable conditions with respect to the production of IEPOX-derived PM in central Amazonia (i.e., lowest NO_y and highest sulfate), f exceeded 0.40 at 25 % frequency. The implication is that at all times significant additional pathways for PM production were active. This conclusion is subject to the accuracy of the IEPOX-SOA factor loading as a scalar proxy of IEPOX-derived PM concentration (see discussion of Fig. 1 in Sect. 3.1). The magnitude of the decrease in f for high sulfate concentrations suggests that IEPOX-derived PM shifted from being a major to a minor component of the PM. Taken together, the results shown in Fig. 7 demonstrate how urban pollution affected the production and composition of regional IEPOX-derived PM.

The data sets presented in Figs. 5, 6, and 7 lead to the conclusion that the additional NO concentrations contributed by Manaus emissions typically suppress the production of IEPOX-derived PM to a greater extent than the additional sulfate concentrations enhance it. Figure 8 presents a systematic visualization. The factor loadings at T3 are represented as contours for axes of sulfate and NO_y concentrations. Higher factor loadings are favored for higher sulfate and lower NO_y concentrations. Factor loadings are most sensitive to changing concentration in the high-sulfate, low-NO_y region. The gray dashed line in Fig. 8 represents a qualitative divisor between domains of typical background and polluted conditions downwind of Manaus.

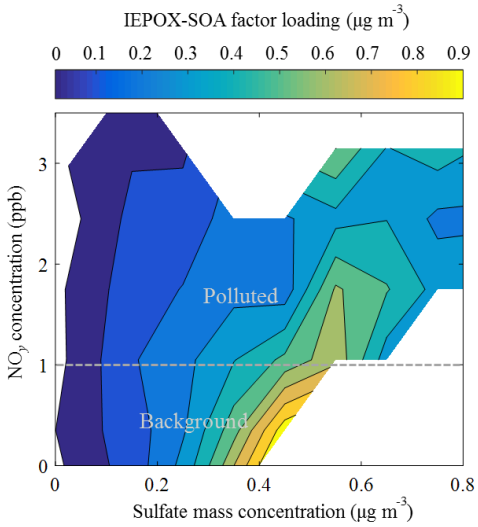

Figure 8. Contours of IEPOX-SOA factor loading for sulfate and NO_y concentrations. The plotted data were recorded during local afternoon (12:00–16:00 local time; 16:00–20:00 UTC). Typical transition between regimes of background and polluted conditions for the region downwind of Manaus are approximately represented by the dashed gray line.

3.5 Influence of NO on production and loss processes of IEPOX-derived PM

Elevated NO concentrations may affect both the production and loss processes of IEPOX-derived PM. On the one hand, production may be reduced because of increased scavenging of ISOPOO by NO, thus obviating production of IEPOX and consequently of IEPOX-derived PM. Production may also be reduced because of more rapid gas-phase loss of IEPOX in response to elevated OH and O_3 concentrations. On the other hand, loss of IEPOX-derived PM may be enhanced due to faster processing of its characteristic compounds by the elevated oxidant concentrations.

A Lagrangian model is employed to help delineate the relative importance of reduced production compared to enhanced loss on the observed IEPOX-derived PM concentrations. The model is initialized by background air that passes over Manaus in the mid-morning. The evolution of IEPOX-derived PM in that air mass is modeled under either polluted or background conditions for arrival at the T3 site in the afternoon. The governing differential equation of the model represents the sum of production and loss processes affecting the concentrations of IEPOX-derived PM, as follows:

$$\frac{\mathrm{d}M}{\mathrm{d}t} = -\alpha_{\mathrm{L}} k_{\mathrm{L}} M + \alpha_{\mathrm{P}} k_{\mathrm{P}}, \quad (1)$$

where M designates the IEPOX-derived PM mass concentration, t designates time, and the first and second terms on the right-hand side represent loss and production processes, respectively. Table 2 lists other symbol definitions and units.

Table 2. Descriptions and units of symbols in the model.

Symbol	Description	Unit
M	Mass concentration of IEPOX-derived PM	$\mu g\,m^{-3}$
t	Time	h
k_P	Zero-order rate coefficient for production under background conditions	$\mu g\,m^{-3}\,h^{-1}$
k_L	First-order rate coefficient for loss under background conditions	h^{-1}
α	Multiplicative factor representing the effects of Manaus pollution on rate coefficients	
τ	Characteristic time of a process (e.g., production, loss, or transport)	h
Subscript tr	Refers to transport	
Subscript bg	Refers to background conditions	
Subscript pol	Refers to polluted conditions	
Subscript 0	Refers to an initial state (i.e., just upwind of Manaus)	
Subscript P	Refers to production processes	
Subscript L	Refers to loss processes	

The analytic solution of Eq. (1) for time t is presented in the Supplement (Sect. S6). From this solution, characteristic times τ for production and loss processes for polluted compared to background conditions are as follows: $\tau_{P,pol} = M_0/(\alpha_P k_P)$, $\tau_{P,bg} = M_0/k_P$, $\tau_{L,pol} = 1/(\alpha_L k_L)$, and $\tau_{L,bg} = 1/k_L$ (Supplement, Sect. S6). The term M_0 represents the IEPOX-derived PM mass concentration just upwind of Manaus. Under background conditions, the enhancement factors α_L and α_P are unity by definition. Under polluted conditions, $\alpha_L = 2$ and $\alpha_P = 0.1$ to reflect enhanced loss and decreased production, respectively. Further descriptions of the model and assumptions are presented in the Supplement (Sect. S6).

The analysis strategy is to compare τ_P and τ_L to the transport time τ_{tr} under polluted and background conditions. In this way, the analysis assesses the relative importance of altered production and loss processes for IEPOX-derived PM from Manaus to T3. The statistical mode value for τ_{tr} of 4 h based on trajectory analysis is used in the model (Martin et al., 2016a). Intervals for the characteristic times τ_P and τ_L are constrained by the T3 afternoon data sets. Concentration ratios ξ, defined as $\xi = M_{pol}/M_{bg}$, are used to constrain the model (Table 3). The quantities M_{pol} and M_{bg} denote $M(t = \tau_{tr})$, meaning the mass concentration at T3 under polluted or background conditions, respectively. The use of the ratio quantity ξ in the analysis, rather than absolute concentrations, provides increased robustness because of low variability in ξ across the observed range of sulfate concentrations, even as M_{pol} and M_{bg} vary greatly (Table 3). The possible impacts of over- or underestimates of IEPOX-derived PM mass concentration, as a consequence of using IEPOX-SOA factor loading as a surrogate, are also mitigated by the use of ξ.

Two cases of the model (1 and 2) are presented, respectively focusing on constraining k_P or k_L and consequently τ_P or τ_L (Table 4). The results for Case 1 of the analysis are shown in Fig. 9a. The value of k_P is varied from 0 to $0.2\,\mu g\,m^{-3}\,h^{-1}$, and the other model parameters are held constant. The loss rate coefficient k_L is fixed at $0.015\,h^{-1}$, corresponding to a characteristic time of 2.8 days (Supplement, Sect. S6). Based on observed values of ξ (gray shaded area in Fig. 9a), an interval for k_P of $[0.07, 0.13]\,\mu g\,m^{-3}\,h^{-1}$ is obtained, as indicated by the vertical dashed lines. Across this interval, M_{bg} and M_{pol} vary from 0.49 to $0.72\,\mu g\,m^{-3}$ and 0.23 to $0.25\,\mu g\,m^{-3}$, respectively, which are consistent with the observed IEPOX-SOA factor loadings (Table 3). The modeled production times have intervals of [1.8, 3.3] h for $\tau_{P,bg}$ and [18, 33] h for $\tau_{P,pol}$.

Case 2 of the analysis evaluates constraints on the loss rate coefficient k_L, and results are shown in Fig. 9b. Loss processes can include chemistry, such as heterogeneous oxidation or other in-particle reactions that reduce the IEPOX-SOA factor loading, as well as physical mechanisms, such as particle deposition and particle dilution by entrainment that reduce mass concentrations of IEPOX-derived PM (Supplement, Sect. S6). The value of k_L is varied over 3 orders of magnitude, representing characteristic times of hours to weeks, and the other model parameters are held constant (Table 4). The production rate coefficient k_P is fixed at $0.10\,\mu g\,m^{-3}\,h^{-1}$, corresponding to the interval midpoint of Case 1. The observed values of ξ (gray shaded area) in intersection with the modeled values of ξ imply an upper limit on k_L at $0.043\,h^{-1}$, corresponding to characteristic times of a day to weeks (Fig. 9b). Correspondingly, $\tau_{L,bg} > 24$ h under background conditions, and $\tau_{L,pol} > 12$ h under polluted conditions.

The analyses of cases 1 and 2 constrain the values of $\tau_{P,pol}$, $\tau_{P,bg}$, $\tau_{L,pol}$, and $\tau_{L,bg}$ based on the observed values of ξ. The lower limits of the characteristic times for loss, meaning $\tau_{L,bg} > 24$ h and $\tau_{L,pol} > 12$ h, are considerably longer than the transport time of 4 h under both background and polluted conditions. Enhanced loss, therefore, does not explain alone the observed values of ξ. By comparison, the observed values of ξ imply a shift in the characteristic time for production from [1.8, 3.3] h under background conditions to [18, 33] h under pollution conditions. The shift in timescale

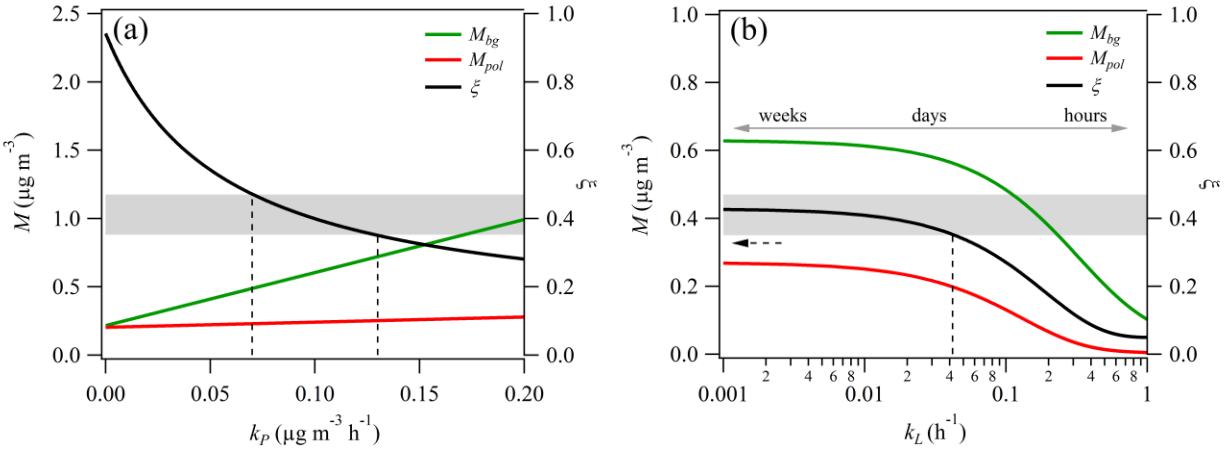

Figure 9. Modeled IEPOX-derived PM mass concentrations M_{pol} and M_{bg} at the T3 site under polluted compared to background conditions. The ratio ξ of concentrations (i.e., M_{pol}/M_{bg}) is also plotted. Panels **(a, b)** correspond to Case 1 and Case 2 listed in Table 4. Gray shading indicates the range of observed values of ξ across low and high sulfate concentrations. Dashed lines indicate the intersection of modeled and observed values of ξ and the corresponding constrained values of k_P or k_L along the abscissa. Labels above the double-headed arrow in **(b)** correspond to characteristic times (i.e., k_L^{-1}). The dashed black arrow in **(b)** communicates that the observed values of ξ provide no constraint on the lower limit of k_L.

Table 3. Interquartile intervals of IEPOX-SOA factor loadings observed for background and polluted conditions. Background and polluted conditions correspond to approximately 0.5 and 2 ppb of NO_y, respectively. The table also lists the resulting ratio ξ of the median factor loading under polluted compared to background conditions.

	Loading (µg m^{-3}) for background conditions		Loading (µg m^{-3}) for polluted conditions		Ratio ξ	
	Low sulfate	High sulfate	Low sulfate	High sulfate	Low sulfate	High sulfate
IEPOX-SOA factor	[0.037, 0.093]	[0.57, 0.95]	[0.022, 0.039]	[0.21, 0.35]	0.47	0.35

Table 4. Parameter values and initial conditions used for the model cases. Descriptions and units are listed in Table 2. The M_0 value is based on the mean IEPOX-SOA factor loading that was measured from 14:00 to 16:00 UTC (10:00–12:00 local time) at a regional background site during 2 months of the wet season in 2008 (Chen et al., 2015). For comparison, a similar value of 0.19 µg m^{-3} was observed during the present study as the mean at the T3 site for $NO_y < 1$ ppb (14:00–16:00 UTC).

Model case	Parameter values				Initial condition
	k_P	k_L	α_P	α_L	M_0
1. Vary k_P	0 to 0.2	0.018	0.1	3	0.23
2. Vary k_L	0.065	0.001 to 1	0.1	3	0.23

is significant in light of the transport time of 4 h. Therefore, reduced production, rather than enhanced loss, is consistent with the lower IEPOX-derived PM concentrations under polluted conditions. A few afternoon hours of altered isoprene chemistry is sufficient to significantly shift the atmospheric concentration of IEPOX-derived PM.

4 Summary and conclusions

The influence of anthropogenic emissions on the production of organic particulate matter from isoprene epoxydiols was studied during the wet season of the tropical forest in central Amazonia. The IEPOX-derived PM concentration at the T3 site, as indicated by the IEPOX-SOA factor loading, was lower under polluted compared to background conditions. Sulfate concentration was an important first-order predictor of the IEPOX-SOA factor loading, corroborating the understanding of the role of sulfate in the production of IEPOX-derived PM that has been developed in laboratory studies as well as in investigations in the southeastern USA (Surratt et al., 2007b; Budisulistiorini et al., 2013, 2015; Hu et al., 2015; Kuwata et al., 2015; Xu et al., 2015). Unlike the southeastern USA, however, where anthropogenic influences dominated variability in sulfate concentrations, contributions by the Manaus urban region to sulfate concentrations were of approximately equal magnitude to the background variability in central Amazonia. By comparison, Manaus urban emissions of NO dominated over background concentrations, and

the NO_y concentration measured 4 to 6 h downwind of Manaus at the T3 site was an important predictor of the IEPOX-SOA factor loading. In net effect, the suppression of IEPOX production because of elevated NO concentrations in the pollution plume dominated over any enhancements in IEPOX uptake because of greater sulfate concentrations.

The dependence of the IEPOX-SOA factor loadings on both sulfate and NO_y concentrations, as shown in Fig. 8, suggests that altered net anthropogenic effects may be expected for different geographic regions, even within Amazonia, and different time periods, such as the wet and dry seasons. The T3 site experienced a wide range of NO_y concentrations, allowing for the systematic demonstration of the dependence of IEPOX-derived PM concentrations on NO_y concentrations. The results show that the transition in isoprene photochemistry related to the production of IEPOX-derived PM is most sensitive precisely at the transition between background and polluted conditions, around 1 ppb of NO_y, at least for central Amazonia in the wet season. These findings suggest that the fraction of PM derived from IEPOX might be lower and have lower variability for other geographic regions characterized by higher NO_y baseline concentrations (e.g., upward of 1 to 2 ppb). For regions further downwind of the urban center, the effects of the plume are expected to phase out both due to dilution and to consumption of NO, and a gradual transition to background chemistry is expected to take place. Adequately representing background conditions and the transition to polluted conditions within models, including the dependence of the production of IEPOX-derived PM not only on sulfate but also on NO concentration, is thus important for making accurate predictions of PM concentrations, both in Amazonia and around the globe.

The findings herein can be considered in the context of Amazonia in transition (Davidson et al., 2012). In the past 50 years, the metropolitan area of Manaus, today at more than 2 million inhabitants, has experienced rapid economic and population growth (Martin et al., 2016a). Changes in the fuel matrix, such as the ongoing shift from high-sulfur to low-sulfur oil in the vehicle fleet as well as from fuel oil to natural gas in many power plants (Medeiros et al., 2017), are changing the composition of the Manaus pollution plume. Based on the findings presented herein, a reduction in sulfate sources from Manaus, whether primary or secondary, would not be expected to considerably affect the mass concentration of IEPOX-derived species in forest regions affected by the plume. Background sources independent of Manaus appear sufficient to sustain sulfate concentrations regionally. In the absence of pollution-control technologies, however, NO emissions can be expected to increase in coming years due to the development of more efficient (i.e., higher temperature) sources of electricity associated with the development of natural gas resources in the basin, as well as from growth in transportation associated with increased population. Increased NO concentrations can be expected to reduce the mass concentration of IEPOX-derived species in forest regions affected by the plume. Changes in the atmospheric particle population can have follow-up effects on cloud type, duration, and rainfall (Pöschl et al., 2010). In addition to PM derived from IEPOX as discussed herein, a better understanding of other pathways that also contribute to organic PM, as well as possible changes to those pathways with increasing pollution in the region, warrants further study so as to achieve sufficient knowledge for decision-making related to air quality and climate in Amazonia.

Data availability. The data sets used in this publication are available at the ARM Climate Research Facility database for the GoAmazon2014/5 experiment (https://www.arm.gov/research/campaigns/amf2014goamazon).

The Supplement related to this article is available online at https://doi.org/10.5194/acp-17-6611-2017-supplement.

Competing interests. The authors declare that they have no conflict of interest.

Acknowledgements. Institutional support was provided by the Central Office of the Large Scale Biosphere Atmosphere Experiment in Amazonia (LBA), the National Institute of Amazonian Research (INPA), and Amazonas State University (UEA). We acknowledge support from the Atmospheric Radiation Measurement (ARM) Climate Research Facility, a user facility of the United States Department of Energy (DOE), Office of Science, sponsored by the Office of Biological and Environmental Research, and support from the Atmospheric System Research (ASR) program of that office. Additional funding was provided by the Amazonas State Research Foundation (FAPEAM), the São Paulo State Research Foundation (FAPESP), the USA National Science Foundation (NSF), and the Brazilian Scientific Mobility Program (CsF/CAPES). S. de Sá acknowledges support by the Schlumberger Foundation, Faculty for the Future Fellowship. The research was conducted under scientific license 001030/2012-4 of the Brazilian National Council for Scientific and Technological Development (CNPq).

Edited by: T. Karl
Reviewed by: two anonymous referees

References

Andreae, M., Berresheim, H., Bingemer, H., Jacob, D. J., Lewis, B., Li, S. M., and Talbot, R. W.: The atmospheric sulfur cycle over the Amazon Basin: 2. Wet season, J. Geophys. Res.-Atmos., 95, 16813–16824, https://doi.org/10.1029/JD095iD10p16813, 1990.

Andreae, M. O., Acevedo, O. C., Araùjo, A., Artaxo, P., Barbosa, C. G. G., Barbosa, H. M. J., Brito, J., Carbone, S., Chi, X., Cintra, B. B. L., da Silva, N. F., Dias, N. L., Dias-Júnior, C. Q., Ditas, F., Ditz, R., Godoi, A. F. L., Godoi, R. H. M., Heimann, M., Hoffmann, T., Kesselmeier, J., Könemann, T., Krüger, M. L., Lavric,

J. V., Manzi, A. O., Lopes, A. P., Martins, D. L., Mikhailov, E. F., Moran-Zuloaga, D., Nelson, B. W., Nölscher, A. C., Santos Nogueira, D., Piedade, M. T. F., Pöhlker, C., Pöschl, U., Quesada, C. A., Rizzo, L. V., Ro, C.-U., Ruckteschler, N., Sá, L. D. A., de Oliveira Sá, M., Sales, C. B., dos Santos, R. M. N., Saturno, J., Schöngart, J., Sörgel, M., de Souza, C. M., de Souza, R. A. F., Su, H., Targhetta, N., Töta, J., Trebs, I., Trumbore, S., van Eijck, A., Walter, D., Wang, Z., Weber, B., Williams, J., Winderlich, J., Wittmann, F., Wolff, S., and Yáñez-Serrano, A. M.: The Amazon Tall Tower Observatory (ATTO): overview of pilot measurements on ecosystem ecology, meteorology, trace gases, and aerosols, Atmos. Chem. Phys., 15, 10723–10776, https://doi.org/10.5194/acp-15-10723-2015, 2015.

Bakwin, P. S., Wofsy, S. C., Fan, S. M., Keller, M., Trumbore, S. E., and Da Costa, J. M.: Emission of nitric oxide (NO) from tropical forest soils and exchange of NO between the forest canopy and atmospheric boundary layers, J. Geophys. Res.-Atmos., 95, 16755–16764, https://doi.org/10.1029/JD095iD10p16755, 1990.

Bateman, A. P., Gong, Z., Liu, P., Sato, B., Cirino, G., Zhang, Y., Artaxo, P., Bertram, A. K., Manzi, A. O., Rizzo, L. V., Souza, R. A. F., Zaveri, R. A., and Martin, S. T.: Sub-micrometre particulate matter is primarily in liquid form over Amazon rainforest, Nat. Geosci., 9, 34–37, https://doi.org/10.1038/ngeo2599, 2016.

Budisulistiorini, S. H., Canagaratna, M. R., Croteau, P. L., Marth, W. J., Baumann, K., Edgerton, E. S., Shaw, S. L., Knipping, E. M., Worsnop, D. R., Jayne, J. T., Gold, A., and Surratt, J. D.: Real-time continuous characterization of secondary organic aerosol derived from isoprene epoxydiols in downtown Atlanta, Georgia, using the Aerodyne Aerosol Chemical Speciation Monitor, Environ. Sci. Technol., 47, 5686–5694, https://doi.org/10.1021/es400023n, 2013.

Budisulistiorini, S. H., Li, X., Bairai, S. T., Renfro, J., Liu, Y., Liu, Y. J., McKinney, K. A., Martin, S. T., McNeill, V. F., Pye, H. O. T., Nenes, A., Neff, M. E., Stone, E. A., Mueller, S., Knote, C., Shaw, S. L., Zhang, Z., Gold, A., and Surratt, J. D.: Examining the effects of anthropogenic emissions on isoprene-derived secondary organic aerosol formation during the 2013 Southern Oxidant and Aerosol Study (SOAS) at the Look Rock, Tennessee ground site, Atmos. Chem. Phys., 15, 8871–8888, https://doi.org/10.5194/acp-15-8871-2015, 2015.

Budisulistiorini, S. H., Baumann, K., Edgerton, E. S., Bairai, S. T., Mueller, S., Shaw, S. L., Knipping, E. M., Gold, A., and Surratt, J. D.: Seasonal characterization of submicron aerosol chemical composition and organic aerosol sources in the southeastern United States: Atlanta, Georgia,and Look Rock, Tennessee, Atmos. Chem. Phys., 16, 5171–5189, https://doi.org/10.5194/acp-16-5171-2016, 2016.

Canagaratna, M. R., Jayne, J. T., Jimenez, J. L., Allan, J. D., Alfarra, M. R., Zhang, Q., Onasch, T. B., Drewnick, F., Coe, H., Middlebrook, A., Delia, A., Williams, L. R., Trimborn, A. M., Northway, M. J., DeCarlo, P. F., Kolb, C. E., Davidovits, P., and Worsnop, D. R.: Chemical and microphysical characterization of ambient aerosols with the aerodyne aerosol mass spectrometer, Mass Spectrom. Rev., 26, 185–222, https://doi.org/10.1002/mas.20115, 2007.

Carbone, S., Brito, J. F., Xu, L., Ng, N. L., Rizzo, L., Cirino, G., Holanda, B., Wolff, S., Saturno, J., Chi, X., Souza, R. A. F., Arana, A., de Sá., M., Krüger, M., Andreae, M. O., Pöhlker, C., Barbosa, H. M. J., and Artaxo, P.: Long-term chemical composition and source apportionment of submicron aerosol particles in the central Amazon basin (ATTO), in preparation, 2017.

Carlton, A. G., Wiedinmyer, C., and Kroll, J. H.: A review of Secondary Organic Aerosol (SOA) formation from isoprene, Atmos. Chem. Phys., 9, 4987–5005, https://doi.org/10.5194/acp-9-4987-2009, 2009.

Chen, Q., Farmer, D. K., Schneider, J., Zorn, S. R., Heald, C. L., Karl, T. G., Guenther, A., Allan, J. D., Robinson, N., Coe, H., Kimmel, J. R., Pauliquevis, T., Borrmann, S., Pöschl, U., Andreae, M. O., Artaxo, P., Jimenez, J. L., and Martin, S. T.: Mass spectral characterization of submicron biogenic organic particles in the Amazon Basin, Geophys. Res. Lett., 36, L20806, https://doi.org/10.1029/2009GL039880, 2009.

Chen, Q., Farmer, D. K., Rizzo, L. V., Pauliquevis, T., Kuwata, M., Karl, T. G., Guenther, A., Allan, J. D., Coe, H., Andreae, M. O., Pöschl, U., Jimenez, J. L., Artaxo, P., and Martin, S. T.: Submicron particle mass concentrations and sources in the Amazonian wet season (AMAZE-08), Atmos. Chem. Phys., 15, 3687–3701, https://doi.org/10.5194/acp-15-3687-2015, 2015.

Claeys, M., Graham, B., Vas, G., Wang, W., Vermeylen, R., Pashynska, V., Cafmeyer, J., Guyon, P., Andreae, M. O., Artaxo, P., and Maenhaut, W.: Formation of secondary organic aerosols through photooxidation of isoprene, Science, 303, 1173–1176, https://doi.org/10.1126/science.1092805, 2004.

Crounse, J. D., Paulot, F., Kjaergaard, H. G., and Wennberg, P. O.: Peroxy radical isomerization in the oxidation of isoprene, Phys. Chem. Chem. Phys., 13, 13607–13613, https://doi.org/10.1039/C1CP21330J, 2011.

Davidson, E. A., de Araújo, A. C., Artaxo, P., Balch, J. K., Brown, I. F., Bustamante, M. M., Coe, M. T., DeFries, R. S., Keller, M., and Longo, M.: The Amazon basin in transition, Nature, 481, 321–328, 2012.

DeCarlo, P. F., Kimmel, J. R., Trimborn, A., Northway, M. J., Jayne, J. T., Aiken, A. C., Gonin, M., Fuhrer, K., Horvath, T., Docherty, K. S., Worsnop, D. R., and Jimenez, J. L.: Field-deployable, high-resolution, time-of-flight aerosol mass spectrometer, Anal. Chem., 78, 8281–8289, https://doi.org/10.1021/ac061249n, 2006.

de Sá, S. S.: Anthropogenic emissions affect the sources and composition of submicron particulate matter in central Amazonia in the wet season, in preparation, 2017.

Ervens, B. and Volkamer, R.: Glyoxal processing by aerosol multiphase chemistry: towards a kinetic modeling framework of secondary organic aerosol formation in aqueous particles, Atmos. Chem. Phys., 10, 8219–8244, https://doi.org/10.5194/acp-10-8219-2010, 2010.

Ervens, B., Turpin, B. J., and Weber, R. J.: Secondary organic aerosol formation in cloud droplets and aqueous particles (aqSOA): a review of laboratory, field and model studies, Atmos. Chem. Phys., 11, 11069–11102, https://doi.org/10.5194/acp-11-11069-2011, 2011.

Fu, T. M., Jacob, D. J., Wittrock, F., Burrows, J. P., Vrekoussis, M., and Henze, D. K.: Global budgets of atmospheric glyoxal and methylglyoxal, and implications for formation of secondary organic aerosols, J. Geophys. Res.-Atmos., 113, D15303, https://doi.org/10.1029/2007JD009505, 2008.

Gaston, C. J., Riedel, T. P., Zhang, Z., Gold, A., Surratt, J. D., and Thornton, J. A.: Reactive uptake of an isoprene-derived epoxy-

diol to submicron aerosol particles, Environ. Sci. Technol., 48, 11178–11186, https://doi.org/10.1021/es5034266, 2014.

Guenther, A. B., Jiang, X., Heald, C. L., Sakulyanontvittaya, T., Duhl, T., Emmons, L. K., and Wang, X.: The Model of Emissions of Gases and Aerosols from Nature version 2.1 (MEGAN2.1): an extended and updated framework for modeling biogenic emissions, Geosci. Model Dev., 5, 1471–1492, https://doi.org/10.5194/gmd-5-1471-2012, 2012.

Hallquist, M., Wenger, J. C., Baltensperger, U., Rudich, Y., Simpson, D., Claeys, M., Dommen, J., Donahue, N. M., George, C., Goldstein, A. H., Hamilton, J. F., Herrmann, H., Hoffmann, T., Iinuma, Y., Jang, M., Jenkin, M. E., Jimenez, J. L., Kiendler-Scharr, A., Maenhaut, W., McFiggans, G., Mentel, Th. F., Monod, A., Prévôt, A. S. H., Seinfeld, J. H., Surratt, J. D., Szmigielski, R., and Wildt, J.: The formation, properties and impact of secondary organic aerosol: current and emerging issues, Atmos. Chem. Phys., 9, 5155–5236, https://doi.org/10.5194/acp-9-5155-2009, 2009.

Hu, W. W., Campuzano-Jost, P., Palm, B. B., Day, D. A., Ortega, A. M., Hayes, P. L., Krechmer, J. E., Chen, Q., Kuwata, M., Liu, Y. J., de Sá, S. S., McKinney, K., Martin, S. T., Hu, M., Budisulistiorini, S. H., Riva, M., Surratt, J. D., St. Clair, J. M., Isaacman-Van Wertz, G., Yee, L. D., Goldstein, A. H., Carbone, S., Brito, J., Artaxo, P., de Gouw, J. A., Koss, A., Wisthaler, A., Mikoviny, T., Karl, T., Kaser, L., Jud, W., Hansel, A., Docherty, K. S., Alexander, M. L., Robinson, N. H., Coe, H., Allan, J. D., Canagaratna, M. R., Paulot, F., and Jimenez, J. L.: Characterization of a real-time tracer for isoprene epoxydiols-derived secondary organic aerosol (IEPOX-SOA) from aerosol mass spectrometer measurements, Atmos. Chem. Phys., 15, 11807–11833, https://doi.org/10.5194/acp-15-11807-2015, 2015.

Hu, W., Palm, B. B., Day, D. A., Campuzano-Jost, P., Krechmer, J. E., Peng, Z., de Sá, S. S., Martin, S. T., Alexander, M. L., Baumann, K., Hacker, L., Kiendler-Scharr, A., Koss, A. R., de Gouw, J. A., Goldstein, A. H., Seco, R., Sjostedt, S. J., Park, J.-H., Guenther, A. B., Kim, S., Canonaco, F., Prévôt, A. S. H., Brune, W. H., and Jimenez, J. L.: Volatility and lifetime against OH heterogeneous reaction of ambient isoprene-epoxydiols-derived secondary organic aerosol (IEPOX-SOA), Atmos. Chem. Phys., 16, 11563–11580, https://doi.org/10.5194/acp-16-11563-2016, 2016.

Isaacman, G., Kreisberg, N. M., Yee, L. D., Worton, D. R., Chan, A. W. H., Moss, J. A., Hering, S. V., and Goldstein, A. H.: Online derivatization for hourly measurements of gas- and particle-phase semi-volatile oxygenated organic compounds by thermal desorption aerosol gas chromatography (SV-TAG), Atmos. Meas. Tech., 7, 4417–4429, https://doi.org/10.5194/amt-7-4417-2014, 2014.

Isaacman-VanWertz, G., Yee, L. D., Kreisberg, N. M., Wernis, R., Moss, J. A., Hering, S. V., de Sá, S. S., Martin, S. T., Alexander, M. L., Palm, B. B., Hu, W., Campuzano-Jost, P., Day, D. A., Jimenez, J. L., Riva, M., Surratt, J. D., Viegas, J., Manzi, A., Edgerton, E., Baumann, K., Souza, R., Artaxo, P., and Goldstein, A. H.: Ambient Gas-Particle Partitioning of Tracers for Biogenic Oxidation, Environ. Sci. Technol., 50, 9952–9962, https://doi.org/10.1021/acs.est.6b01674, 2016.

Jacob, D. J. and Wofsy, S. C.: Budgets of reactive nitrogen, hydrocarbons, and ozone over the Amazon forest during the wet season, J. Geophys. Res.-Atmos., 95, 16737–16754, https://doi.org/10.1029/JD095iD10p16737, 1990.

Jacobs, M. I., Burke, W. J., and Elrod, M. J.: Kinetics of the reactions of isoprene-derived hydroxynitrates: gas phase epoxide formation and solution phase hydrolysis, Atmos. Chem. Phys., 14, 8933–8946, https://doi.org/10.5194/acp-14-8933-2014, 2014.

Jimenez, J. L., Canagaratna, M. R., Donahue, N. M., Prevot, A. S. H., Zhang, Q., Kroll, J. H., DeCarlo, P. F., Allan, J. D., Coe, H., Ng, N. L., Aiken, A. C., Docherty, K. S., Ulbrich, I. M., Grieshop, A. P., Robinson, A. L., Duplissy, J., Smith, J. D., Wilson, K. R., Lanz, V. A., Hueglin, C., Sun, Y. L., Tian, J., Laaksonen, A., Raatikainen, T., Rautiainen, J., Vaattovaara, P., Ehn, M., Kulmala, M., Tomlinson, J. M., Collins, D. R., Cubison, M. J., Dunlea, J., Huffman, J. A., Onasch, T. B., Alfarra, M. R., Williams, P. I., Bower, K., Kondo, Y., Schneider, J., Drewnick, F., Borrmann, S., Weimer, S., Demerjian, K., Salcedo, D., Cottrell, L., Griffin, R., Takami, A., Miyoshi, T., Hatakeyama, S., Shimono, A., Sun, J. Y., Zhang, Y. M., Dzepina, K., Kimmel, J. R., Sueper, D., Jayne, J. T., Herndon, S. C., Trimborn, A. M., Williams, L. R., Wood, E. C., Middlebrook, A. M., Kolb, C. E., Baltensperger, U., and Worsnop, D. R.: Evolution of organic aerosols in the atmosphere, Science, 326, 1525–1529, https://doi.org/10.1126/science.1180353, 2009.

Kanakidou, M., Seinfeld, J. H., Pandis, S. N., Barnes, I., Dentener, F. J., Facchini, M. C., Van Dingenen, R., Ervens, B., Nenes, A., Nielsen, C. J., Swietlicki, E., Putaud, J. P., Balkanski, Y., Fuzzi, S., Horth, J., Moortgat, G. K., Winterhalter, R., Myhre, C. E. L., Tsigaridis, K., Vignati, E., Stephanou, E. G., and Wilson, J.: Organic aerosol and global climate modelling: a review, Atmos. Chem. Phys., 5, 1053–1123, https://doi.org/10.5194/acp-5-1053-2005, 2005.

Kaufman, Y. J., Tanré, D., and Boucher, O.: A satellite view of aerosols in the climate system, Nature, 419, 215–223, 2002.

Kjaergaard, H. G., Knap, H. C., Ørnsø, K. B., Jørgensen, S., Crounse, J. D., Paulot, F., and Wennberg, P. O.: Atmospheric Fate of Methacrolein. 2. Formation of Lactone and Implications for Organic Aerosol Production, J. Phys. Chem. A, 116, 5763–5768, https://doi.org/10.1021/jp210853h, 2012.

Krechmer, J. E., Coggon, M. M., Massoli, P., Nguyen, T. B., Crounse, J. D., Hu, W., Day, D. A., Tyndall, G. S., Henze, D. K., Rivera-Rios, J. C., Nowak, J. B., Kimmel, J. R., Mauldin, R. L., Stark, H., Jayne, J. T., Sipilä, M., Junninen, H., Clair, J. M. S., Zhang, X., Feiner, P. A., Zhang, L., Miller, D. O., Brune, W. H., Keutsch, F. N., Wennberg, P. O., Seinfeld, J. H., Worsnop, D. R., Jimenez, J. L., and Canagaratna, M. R.: Formation of low volatility organic compounds and secondary organic aerosol from isoprene hydroxyhydroperoxide low-NO oxidation, Environ. Sci. Technol., 49, 10330–10339, https://doi.org/10.1021/acs.est.5b02031, 2015.

Kroll, J. H., Ng, N. L., Murphy, S. M., Flagan, R. C., and Seinfeld, J. H.: Secondary organic aerosol formation from isoprene photooxidation under high-NO_x conditions, Geophys. Res. Lett., 32, L18808, https://doi.org/10.1029/2005GL023637, 2005.

Kuhn, U., Ganzeveld, L., Thielmann, A., Dindorf, T., Schebeske, G., Welling, M., Sciare, J., Roberts, G., Meixner, F. X., Kesselmeier, J., Lelieveld, J., Kolle, O., Ciccioli, P., Lloyd, J., Trentmann, J., Artaxo, P., and Andreae, M. O.: Impact of Manaus City on the Amazon Green Ocean atmosphere: ozone production,

precursor sensitivity and aerosol load, Atmos. Chem. Phys., 10, 9251–9282, https://doi.org/10.5194/acp-10-9251-2010, 2010.

Kuwata, M., Liu, Y., McKinney, K., and Martin, S. T.: Physical state and acidity of inorganic sulfate can regulate the production of secondary organic material from isoprene photooxidation products, Phys. Chem. Chem. Phys., 17, 5670–5678, https://doi.org/10.1039/C4CP04942J, 2015.

Levine, J. G., MacKenzie, A. R., Squire, O. J., Archibald, A. T., Griffiths, P. T., Abraham, N. L., Pyle, J. A., Oram, D. E., Forster, G., Brito, J. F., Lee, J. D., Hopkins, J. R., Lewis, A. C., Bauguitte, S. J. B., Demarco, C. F., Artaxo, P., Messina, P., Lathière, J., Hauglustaine, D. A., House, E., Hewitt, C. N., and Nemitz, E.: Isoprene chemistry in pristine and polluted Amazon environments: Eulerian and Lagrangian model frameworks and the strong bearing they have on our understanding of surface ozone and predictions of rainforest exposure to this priority pollutant, Atmos. Chem. Phys. Discuss., 15, 24251–24310, https://doi.org/10.5194/acpd-15-24251-2015, 2015.

Lewandowski, M., Jaoui, M., Offenberg, J. H., Krug, J. D., and Kleindienst, T. E.: Atmospheric oxidation of isoprene and 1,3-butadiene: influence of aerosol acidity and relative humidity on secondary organic aerosol, Atmos. Chem. Phys., 15, 3773–3783, https://doi.org/10.5194/acp-15-3773-2015, 2015.

Lim, H.-J., Carlton, A. G., and Turpin, B. J.: Isoprene forms secondary organic aerosol through cloud processing: Model simulations, Environ. Sci. Technol., 39, 4441–4446, https://doi.org/10.1021/es048039h, 2005.

Lin, Y.-H., Zhang, Z., Docherty, K. S., Zhang, H., Budisulistiorini, S. H., Rubitschun, C. L., Shaw, S. L., Knipping, E. M., Edgerton, E. S., Kleindienst, T. E., Gold, A., and Surratt, J. D.: Isoprene epoxydiols as precursors to secondary organic aerosol formation: acid-catalyzed reactive uptake studies with authentic compounds, Environ. Sci. Technol., 46, 250–258, https://doi.org/10.1021/es202554c, 2012.

Lin, Y.-H., Zhang, H., Pye, H. O. T., Zhang, Z., Marth, W. J., Park, S., Arashiro, M., Cui, T., Budisulistiorini, S. H., Sexton, K. G., Vizuete, W., Xie, Y., Luecken, D. J., Piletic, I. R., Edney, E. O., Bartolotti, L. J., Gold, A., and Surratt, J. D.: Epoxide as a precursor to secondary organic aerosol formation from isoprene photooxidation in the presence of nitrogen oxides, P. Natl. Acad. Sci. USA, 110, 6718–6723, https://doi.org/10.1073/pnas.1221150110, 2013.

Lin, Y.-H., Budisulistiorini, S. H., Chu, K., Siejack, R. A., Zhang, H., Riva, M., Zhang, Z., Gold, A., Kautzman, K. E., and Surratt, J. D.: Light-absorbing oligomer formation in secondary organic aerosol from reactive uptake of isoprene epoxydiols, Environ. Sci. Technol., 48, 12012–12021, https://doi.org/10.1021/es503142b, 2014.

Liu, Y., Kuwata, M., Strick, B. F., Geiger, F. M., Thomson, R. J., McKinney, K. A., and Martin, S. T.: Uptake of epoxydiol isomers accounts for half of the particle-phase material produced from isoprene photooxidation via the HO_2 pathway, Environ. Sci. Technol., 49, 250–258, https://doi.org/10.1021/es5034298, 2015.

Liu, Y., Brito, J., Dorris, M. R., Rivera-Rios, J. C., Seco, R., Bates, K. H., Artaxo, P., Duvoisin, S., Keutsch, F. N., Kim, S., Goldstein, A. H., Guenther, A. B., Manzi, A. O., Souza, R. A. F., Springston, S. R., Watson, T. B., McKinney, K. A., and Martin, S. T.: Isoprene photochemistry over the Amazon rain forest, P. Natl. Acad. Sci. USA, 113, 6125–6130, https://doi.org/10.1073/pnas.1524136113, 2016a.

Liu, J., D'Ambro, E. L., Lee, B. H., Lopez-Hilfiker, F. D., Zaveri, R. A., Rivera-Rios, J. C., Keutsch, F. N., Iyer, S., Kurten, T., Zhang, Z., Gold, A., Surratt, J. D., Shilling, J. E., and Thornton, J. A.: Efficient Isoprene Secondary Organic Aerosol Formation from a Non-IEPOX Pathway, Environ. Sci. Technol., 50, 9872–9880, https://doi.org/10.1021/acs.est.6b01872, 2016b.

Liu, Y., Kuwata, M., McKinney, K. A., and Martin, S. T.: Uptake and release of gaseous species accompanying the reactions of isoprene photo-oxidation products with sulfate particles, Phys. Chem. Chem. Phys., 18, 1595–1600, https://doi.org/10.1039/C5CP04551G, 2016c.

Liu, Y. J., Herdlinger-Blatt, I., McKinney, K. A., and Martin, S. T.: Production of methyl vinyl ketone and methacrolein via the hydroperoxyl pathway of isoprene oxidation, Atmos. Chem. Phys., 13, 5715–5730, https://doi.org/10.5194/acp-13-5715-2013, 2013.

Lopez-Hilfiker, F. D., Mohr, C., D'Ambro, E. L., Lutz, A., Riedel, T. P., Gaston, C. J., Iyer, S., Zhang, Z., Gold, A., Surratt, J. D., Lee, B. H., Kurten, T., Hu, W. W., Jimenez, J., Hallquist, M., and Thornton, J. A.: Molecular composition and volatility of organic aerosol in the Southeastern US: implications for IEPOX derived SOA, Environ. Sci. Technol., 50, 2200–2209, https://doi.org/10.1021/acs.est.5b04769, 2016.

Marais, E. A., Jacob, D. J., Jimenez, J. L., Campuzano-Jost, P., Day, D. A., Hu, W., Krechmer, J., Zhu, L., Kim, P. S., Miller, C. C., Fisher, J. A., Travis, K., Yu, K., Hanisco, T. F., Wolfe, G. M., Arkinson, H. L., Pye, H. O. T., Froyd, K. D., Liao, J., and McNeill, V. F.: Aqueous-phase mechanism for secondary organic aerosol formation from isoprene: application to the southeast United States and co-benefit of SO2 emission controls, Atmos. Chem. Phys., 16, 1603–1618, https://doi.org/10.5194/acp-16-1603-2016, 2016.

Martin, S. T., Andreae, M. O., Artaxo, P., Baumgardner, D., Chen, Q., Goldstein, A. H., Guenther, A., Heald, C. L., Mayol-Bracero, O. L., McMurry, P. H., Pauliquevis, T., Pöschl, U., Prather, K. A., Roberts, G. C., Saleska, S. R., Silva Dias, M. A., Spracklen, D. V., Swietlicki, E., and Trebs, I.: Sources and properties of Amazonian aerosol particles, Rev. Geophys., 48, RG2012, https://doi.org/10.1029/2008RG000280, 2010a.

Martin, S. T., Andreae, M. O., Althausen, D., Artaxo, P., Baars, H., Borrmann, S., Chen, Q., Farmer, D. K., Guenther, A., Gunthe, S. S., Jimenez, J. L., Karl, T., Longo, K., Manzi, A., Müller, T., Pauliquevis, T., Petters, M. D., Prenni, A. J., Pöschl, U., Rizzo, L. V., Schneider, J., Smith, J. N., Swietlicki, E., Tota, J., Wang, J., Wiedensohler, A., and Zorn, S. R.: An overview of the Amazonian Aerosol Characterization Experiment 2008 (AMAZE-08), Atmos. Chem. Phys., 10, 11415–11438, https://doi.org/10.5194/acp-10-11415-2010, 2010b.

Martin, S. T., Artaxo, P., Machado, L. A. T., Manzi, A. O., Souza, R. A. F., Schumacher, C., Wang, J., Andreae, M. O., Barbosa, H. M. J., Fan, J., Fisch, G., Goldstein, A. H., Guenther, A., Jimenez, J. L., Pöschl, U., Silva Dias, M. A., Smith, J. N., and Wendisch, M.: Introduction: Observations and Modeling of the Green Ocean Amazon (GoAmazon2014/5), Atmos. Chem. Phys., 16, 4785–4797, https://doi.org/10.5194/acp-16-4785-2016, 2016a.

Martin, S. T., Artaxo, P. E., Chen, Q., Guenther, A. B., Gunthe, S. S., Jimenez, J. L., Manzi, A., Prenni, K. L., Pöschl, U., Schnei-

der, J., and Swietlicki, E.: AMAZE-08 Aerosol Characterization and Meteorological Data, Central Amazon Basin: 2008, ORNL Distributed Active Archive Center, 2016b.

Martin, S. T., Artaxo, P., Machado, L., Manzi, A. O., Souza, R. A. F., Schumacher, C., Wang, J., Biscaro, T., Brito, J., Calheiros, A., Jardine, K., Medeiros, A., Portela, B., Sá, S. S. d., Adachi, K., Aiken, A. C., Albrecht, R., Alexander, L., Andreae, M. O., Barbosa, H. M. J., Buseck, P., Chand, D., Comstock, J. M., Day, D. A., Dubey, M., Fan, J., Fast, J., Fisch, G., Fortner, E., Giangrande, S., Gilles, M., Goldstein, A. H., Guenther, A., Hubbe, J., Jensen, M., Jimenez, J. L., Keutsch, F. N., Kim, S., Kuang, C., Laskin, A., McKinney, K., Mei, F., Miller, M., Nascimento, R., Pauliquevis, T., Pekour, M., Peres, J., Petäjä, T., Pöhlker, C., Pöschl, U., Rizzo, L., Schmid, B., Shilling, J. E., Dias, M. A. S., Smith, J. N., Tomlinson, J. M., Tóta, J., and Wendisch, M.: The Green ocean Amazon Experiment (GoAmazon2014/5) observes pollution affecting gases, aerosols, clouds, and rainfall over the rain forest, B. Am. Meteorol. Soc., 98, 981–997, https://doi.org/10.1175/BAMS-D-15-00221.1, 2017.

Mather, J. H. and Voyles, J. W.: The ARM Climate Research Facility: A review of structure and capabilities, B. Am. Meteorol. Soc., 94, 377–392, https://doi.org/10.1175/BAMS-D-11-00218.1, 2013.

McNeill, V. F., Woo, J. L., Kim, D. D., Schwier, A. N., Wannell, N. J., Sumner, A. J., and Barakat, J. M.: Aqueous-phase secondary organic aerosol and organosulfate formation in atmospheric aerosols: a modeling study, Environ. Sci. Technol., 46, 8075–8081, https://doi.org/10.1021/es3002986, 2012.

Medeiros, A. S. S., Calderaro, G., Guimarães, P. C., Magalhaes, M. R., Morais, M. V. B., Rafee, S. A. A., Ribeiro, I. O., Andreoli, R. V., Martins, J. A., Martins, L. D., Martin, S. T., and Souza, R. A. F.: Power Plant Fuel Switching and Air Quality in a Tropical Forested Environment, Atmos. Chem. Phys. Discuss., https://doi.org/10.5194/acp-2016-1113, in review, 2017.

Nel, A.: Air pollution-related illness: effects of particles, Science, 308, 804–806, 2005.

Nguyen, T. B., Coggon, M. M., Bates, K. H., Zhang, X., Schwantes, R. H., Schilling, K. A., Loza, C. L., Flagan, R. C., Wennberg, P. O., and Seinfeld, J. H.: Organic aerosol formation from the reactive uptake of isoprene epoxydiols (IEPOX) onto non-acidified inorganic seeds, Atmos. Chem. Phys., 14, 3497–3510, https://doi.org/10.5194/acp-14-3497-2014, 2014.

Nguyen, T. B., Bates, K. H., Crounse, J. D., Schwantes, R. H., Zhang, X., Kjaergaard, H. G., Surratt, J. D., Lin, P., Laskin, A., Seinfeld, J. H., and Wennberg, P. O.: Mechanism of the hydroxyl radical oxidation of methacryloyl peroxynitrate (MPAN) and its pathway toward secondary organic aerosol formation in the atmosphere, Phys. Chem. Chem. Phys., 17, 17914–17926, https://doi.org/10.1039/C5CP02001H, 2015.

Pandis, S. N., Paulson, S. E., Seinfeld, J. H., and Flagan, R. C.: Aerosol formation in the photooxidation of isoprene and β-pinene, Atmos. Environ.-A Gen., 25, 997–1008, https://doi.org/10.1016/0960-1686(91)90141-S, 1991.

Paulot, F., Crounse, J. D., Kjaergaard, H. G., Kürten, A., Clair, J. M. S., Seinfeld, J. H., and Wennberg, P. O.: Unexpected epoxide formation in the gas-phase photooxidation of isoprene, Science, 325, 730–733, https://doi.org/10.1126/science.1172910, 2009.

Pope III, C. A. and Dockery, D. W.: Health effects of fine particulate air pollution: lines that connect, J. Air Waste Manage., 56, 709–742, 2006.

Pöschl, U., Martin, S. T., Sinha, B., Chen, Q., Gunthe, S. S., Huffman, J. A., Borrmann, S., Farmer, D. K., Garland, R. M., Helas, G., Jimenez, J. L., King, S. M., Manzi, A., Mikhailov, E., Pauliquevis, T., Petters, M. D., Prenni, A. J., Roldin, P., Rose, D., Schneider, J., Su, H., Zorn, S. R., Artaxo, P., and Andreae, M. O.: Rainforest aerosols as biogenic nuclei of clouds and precipitation in the Amazon, Science, 329, 1513–1516, https://doi.org/10.1126/science.1191056, 2010.

Ramanathan, V., Crutzen, P., Kiehl, J., and Rosenfeld, D.: Aerosols, climate, and the hydrological cycle, Science, 294, 2119–2124, 2001.

Riedel, T. P., Lin, Y.-H., Zhang, Z., Chu, K., Thornton, J. A., Vizuete, W., Gold, A., and Surratt, J. D.: Constraining condensed-phase formation kinetics of secondary organic aerosol components from isoprene epoxydiols, Atmos. Chem. Phys., 16, 1245–1254, https://doi.org/10.5194/acp-16-1245-2016, 2016.

Riva, M., Bell, D. M., Hansen, A.-M. K., Drozd, G. T., Zhang, Z., Gold, A., Imre, D., Surratt, J. D., Glasius, M., and Zelenyuk, A.: Effect of organic coatings, humidity and aerosol acidity on multiphase chemistry of isoprene epoxydiols, Environ. Sci. Technol., 50, 5580–5588, https://doi.org/10.1021/acs.est.5b06050, 2016a.

Riva, M., Budisulistiorini, S. H., Chen, Y., Zhang, Z., D'Ambro, E. L., Zhang, X., Gold, A., Turpin, B. J., Thornton, J. A., Canagaratna, M. R., and Surratt, J. D.: Chemical characterization of secondary organic aerosol from oxidation of isoprene hydroxyhydroperoxides, Environ. Sci. Technol., 50, 9889–9899, https://doi.org/10.1021/acs.est.6b02511, 2016b.

Robinson, N. H., Hamilton, J. F., Allan, J. D., Langford, B., Oram, D. E., Chen, Q., Docherty, K., Farmer, D. K., Jimenez, J. L., Ward, M. W., Hewitt, C. N., Barley, M. H., Jenkin, M. E., Rickard, A. R., Martin, S. T., McFiggans, G., and Coe, H.: Evidence for a significant proportion of Secondary Organic Aerosol from isoprene above a maritime tropical forest, Atmos. Chem. Phys., 11, 1039–1050, https://doi.org/10.5194/acp-11-1039-2011, 2011.

Rohrer, F., Lu, K., Hofzumahaus, A., Bohn, B., Brauers, T., Chang, C.-C., Fuchs, H., Haseler, R., Holland, F., Hu, M., Kita, K., Kondo, Y., Li, X., Lou, S., Oebel, A., Shao, M., Zeng, L., Zhu, T., Zhang, Y., and Wahner, A.: Maximum efficiency in the hydroxyl-radical-based self-cleansing of the troposphere, Nat. Geosci., 7, 559–563, https://doi.org/10.1038/ngeo2199, 2014.

Romer, P. S., Duffey, K. C., Wooldridge, P. J., Allen, H. M., Ayres, B. R., Brown, S. S., Brune, W. H., Crounse, J. D., de Gouw, J., Draper, D. C., Feiner, P. A., Fry, J. L., Goldstein, A. H., Koss, A., Misztal, P. K., Nguyen, T. B., Olson, K., Teng, A. P., Wennberg, P. O., Wild, R. J., Zhang, L., and Cohen, R. C.: The lifetime of nitrogen oxides in an isoprene-dominated forest, Atmos. Chem. Phys., 16, 7623–7637, https://doi.org/10.5194/acp-16-7623-2016, 2016.

Rummel, U., Ammann, C., Kirkman, G. A., Moura, M. A. L., Foken, T., Andreae, M. O., and Meixner, F. X.: Seasonal variation of ozone deposition to a tropical rain forest in southwest Amazonia, Atmos. Chem. Phys., 7, 5415–5435, https://doi.org/10.5194/acp-7-5415-2007, 2007.

Schmid, B., Tomlinson, J. M., Hubbe, J. M., Comstock, J. M., Mei, F., Chand, D., Pekour, M. S., Kluzek, C. D., Andrews, E., Biraud, S. C., and McFarquhar, G. M.: The DOE ARM aerial facility, B. Am. Meteorol. Soc., 95, 723–742, https://doi.org/10.1175/BAMS-D-13-00040.1, 2014.

Slowik, J. G., Brook, J., Chang, R. Y.-W., Evans, G. J., Hayden, K., Jeong, C.-H., Li, S.-M., Liggio, J., Liu, P. S. K., McGuire, M., Mihele, C., Sjostedt, S., Vlasenko, A., and Abbatt, J. P. D.: Photochemical processing of organic aerosol at nearby continental sites: contrast between urban plumes and regional aerosol, Atmos. Chem. Phys., 11, 2991–3006, https://doi.org/10.5194/acp-11-2991-2011, 2011.

St. Clair, J. M., Rivera-Rios, J. C., Crounse, J. D., Knap, H. C., Bates, K. H., Teng, A. P., Jørgensen, S., Kjaergaard, H. G., Keutsch, F. N., and Wennberg, P. O.: Kinetics and products of the reaction of the first-generation isoprene hydroxy hydroperoxide (ISOPOOH) with OH, J. Phys. Chem. A, 120, 1441–1451, https://doi.org/10.1021/acs.jpca.5b06532, 2015.

Surratt, J. D., Murphy, S. M., Kroll, J. H., Ng, N. L., Hildebrandt, L., Sorooshian, A., Szmigielski, R., Vermeylen, R., Maenhaut, W., Claeys, M., Flagan, R. C., and Seinfeld, J. H.: Chemical composition of secondary organic aerosol formed from the photooxidation of isoprene, J. Phys. Chem. A, 110, 9665–9690, https://doi.org/10.1021/jp061734m, 2006.

Surratt, J. D., Lewandowski, M., Offenberg, J. H., Jaoui, M., Kleindienst, T. E., Edney, E. O., and Seinfeld, J. H.: Effect of acidity on secondary organic aerosol formation from isoprene, Environ. Sci. Technol., 41, 5363–5369, https://doi.org/10.1021/es0704176, 2007a.

Surratt, J. D., Kroll, J. H., Kleindienst, T. E., Edney, E. O., Claeys, M., Sorooshian, A., Ng, N. L., Offenberg, J. H., Lewandowski, M., Jaoui, M., Flagan, R. C., and Seinfeld, J. H.: Evidence for organosulfates in secondary organic aerosol, Environ. Sci. Technol., 41, 517–527, https://doi.org/10.1021/es062081q, 2007b.

Surratt, J. D., Chan, A. W., Eddingsaas, N. C., Chan, M., Loza, C. L., Kwan, A. J., Hersey, S. P., Flagan, R. C., Wennberg, P. O., and Seinfeld, J. H.: Reactive intermediates revealed in secondary organic aerosol formation from isoprene, P. Natl. Acad. Sci. USA, 107, 6640–6645, https://doi.org/10.1073/pnas.0911114107, 2010.

Torres, A. and Buchan, H.: Tropospheric nitric oxide measurements over the Amazon Basin, J. Geophys. Res.-Atmos., 93, 1396–1406, https://doi.org/10.1029/JD093iD02p01396, 1988.

Trebs, I., Mayol-Bracero, O. L., Pauliquevis, T., Kuhn, U., Sander, R., Ganzeveld, L., Meixner, F. X., Kesselmeier, J., Artaxo, P., and Andreae, M. O.: Impact of the Manaus urban plume on trace gas mixing ratios near the surface in the Amazon Basin: Implications for the NO-NO_2-O_3 photostationary state and peroxy radical levels, J. Geophys. Res.-Atmos., 117, D05307, https://doi.org/10.1029/2011JD016386, 2012.

Ulbrich, I. M., Canagaratna, M. R., Zhang, Q., Worsnop, D. R., and Jimenez, J. L.: Interpretation of organic components from Positive Matrix Factorization of aerosol mass spectrometric data, Atmos. Chem. Phys., 9, 2891–2918, https://doi.org/10.5194/acp-9-2891-2009, 2009.

Valin, L., Russell, A., and Cohen, R.: Variations of OH radical in an urban plume inferred from NO_2 column measurements, Geophys. Res. Lett., 40, 1856–1860, https://doi.org/10.1002/grl.50267, 2013.

Volkamer, R., San Martini, F., Molina, L. T., Salcedo, D., Jimenez, J. L., and Molina, M. J.: A missing sink for gas-phase glyoxal in Mexico City: Formation of secondary organic aerosol, Geophys. Res. Lett., 34, L19807, https://doi.org/10.1029/2007GL030752, 2007.

Wang, W., Kourtchev, I., Graham, B., Cafmeyer, J., Maenhaut, W., and Claeys, M.: Characterization of oxygenated derivatives of isoprene related to 2-methyltetrols in Amazonian aerosols using trimethylsilylation and gas chromatography/ion trap mass spectrometry, Rapid. Commun. Mass Sp., 19, 1343–1351, https://doi.org/10.1002/rcm.1940, 2005.

Wennberg, P.: Let's abandon the "high NO_x" and "low NO_x" terminology, IGAC news, 50, 3–4, 2013.

Worton, D. R., Surratt, J. D., LaFranchi, B. W., Chan, A. W. H., Zhao, Y., Weber, R. J., Park, J.-H., Gilman, J. B., de Gouw, J., Park, C., Schade, G., Beaver, M., Clair, J. M. S., Crounse, J., Wennberg, P., Wolfe, G. M., Harrold, S., Thornton, J. A., Farmer, D. K., Docherty, K. S., Cubison, M. J., Jimenez, J.-L., Frossard, A. A., Russell, L. M., Kristensen, K., Glasius, M., Mao, J., Ren, X., Brune, W., Browne, E. C., Pusede, S. E., Cohen, R. C., Seinfeld, J. H., and Goldstein, A. H.: Observational insights into aerosol formation from isoprene, Environ. Sci. Technol., 47, 11403–11413, https://doi.org/10.1021/es4011064, 2013.

Xu, L., Guo, H., Boyd, C. M., Klein, M., Bougiatioti, A., Cerully, K. M., Hite, J. R., Isaacman-VanWertz, G., Kreisberg, N. M., Knote, C., Olson, K., Koss, A., Goldstein, A. H., Hering, S. V., de Gouw, J., Baumann, K., Lee, S.-H., Nenes, A., Weber, R. J., and Ng, N. L.: Effects of anthropogenic emissions on aerosol formation from isoprene and monoterpenes in the southeastern United States, P. Natl. Acad. Sci. USA, 112, 37–42, https://doi.org/10.1073/pnas.1417609112, 2015.

Zhang, Q., Jimenez, J. L., Canagaratna, M. R., Allan, J. D., Coe, H., Ulbrich, I., Alfarra, M. R., Takami, A., Middlebrook, A. M., Sun, Y. L., Dzepina, K., Dunlea, E., Docherty, K., DeCarlo, P. F., Salcedo, D., Onasch, T., Jayne, J. T., Miyoshi, T., Shimono, A., Hatakeyama, S., Takegawa, N., Kondo, Y., Schneider, J., Drewnick, F., Borrmann, S., Weimer, S., Demerjian, K., Williams, P., Bower, K., Bahreini, R., Cottrell, L., Griffin, R. J., Rautiainen, J., Sun, J. Y., Zhang, Y. M., and Worsnop, D. R.: Ubiquity and dominance of oxygenated species in organic aerosols in anthropogenically-influenced Northern Hemisphere midlatitudes, Geophys. Res. Lett., 34, L13801, https://doi.org/10.1029/2007GL029979, 2007.

Supplement of Atmos. Chem. Phys., 17, 6611–6629, 2017
https://doi.org/10.5194/acp-17-6611-2017-supplement

Atmospheric Chemistry and Physics
Open Access
EGU

Supplement of

Influence of urban pollution on the production of organic particulate matter from isoprene epoxydiols in central Amazonia

Suzane S. de Sá et al.

Correspondence to: Scot T. Martin (scot_martin@harvard.edu)

S1. Instrumentation

S1.1 Aerosol Mass Spectrometry: set up and operation

Online measurements of organic and sulfate mass concentrations measured in this study were made by a High-Resolution Time-of-Flight Aerosol Mass Spectrometer (AMS, Aerodyne Research Inc.) (DeCarlo et al., 2006; Canagaratna et al., 2007). The AMS provided real-time measurements of bulk non-refractory particle chemical composition (organic, sulfate, nitrate, ammonium, chloride) and chemically resolved mass-diameter distribution. Air was sampled through a critical orifice and enters an aerodynamic lens, which focused the submicron particles into a narrow beam (Zhang et al., 2004). Particles traveled through a sizing chamber to reach a porous tungsten inverted-cone vaporizer at 600 °C, and non-refractory components volatilized. The gaseous molecules were then ionized through electron impact (70 eV), and the ions were measured by time-of-flight mass spectrometry. The high mass resolution allowed for the distinction of ions having the same nominal mass but different elemental composition. Data analysis was performed using standard AMS software (*SQUIRREL* 1.56D, *PIKA* 1.14G) (webpage: http://cires1.colorado.edu/jimenez-group/ToFAMSResources/ToFSoftware/index.html).

Aerosol particles were sampled through a cyclone (URG-2000-30EH) which had a size cut of 2.5 um for a flow of 16.7 L min^{-1}. The sampled flow (14.9 to 16.3 L min^{-1}) traveled through a stainless steel tube for about 1.5 m. The flow was then split in two: a 4-m line for sampling (1.2 or 2.6 L min^{-1}) and a line (13.7 L min^{-1}) for exhaust. The sampling flow changed between 1.2 and 2.6 L min^{-1} according to the flow set up of the Scanning Mobility Particle Sizer (SMPS), which was sampling in parallel to the AMS. The sampling flow then entered a poly-tube Nafion dryer (Perma Pure, model PD-100T). Drying prior to entering the instrument

container aimed at avoiding water condensation in the line inside the container, which was always kept at lower temperatures than outside (i.e., trailer temperature was around 23 °C during daytime). RH measured after the poly-tube dryer and inside the container was at 40 to 80%. Within the container, a subflow (0.6 or 3 L min^{-1}) was passed through a mono-tube Nafion dryer (Perma Pure, model MD-110) to reach RH < 40%. A flow of 0.09 L min^{-1} was sampled by the AMS, and the remaining flow of 0.5 or 2.9 L min^{-1} was sampled by the SMPS. The ambient air sampling line was integrated to a valve switching system, which alternated the AMS/SMPS sampling between the unprocessed ambient air and air processed by oxidation flow reactors or a thermal denuder. The unprocessed ambient air (used for this analysis) was sampled for 4 out of 8 min, constituting half of the total acquired data set.

Due to expected low mass concentrations and to secondary need for the low-sensitivity high-resolution data, the AMS was operated for most of the time in medium-resolution V-mode ($\Delta m/m$ = 2200 at m/z 44), which was used for mass quantification. High-resolution W-mode ($\Delta m/m$ = 4000 at m/z 44) was acquired for one of every six days. These data were used to aid choice of ions to fit. When only V-mode data were acquired, the instrument was operated in "mass spectrum" sub-mode for 180 s and in "particle-time-of-flight" sub-mode for 60 s. When W-mode data were also collected, the "W-mass-spectrum" sub-mode was operated for 60 s, the "V-mass-spectrum" sub-mode ran for 120 s, and "V-particle-time-of-flight" sub-mode ran for 60 s. Both ways of operation corresponded to 4 min for each cycle, allowing for synchronization to the valve switching system.

The AMS sensitivity and the ammonium relative ionization efficiency (RIE) were calibrated every five days using dried ammonium nitrate particles having a mobility diameter of 400 nm. An interpolated curve of the obtained values, corresponding to RIE = 4.3 ± 0.2, was

used for mass calculation corrections. The sulfate RIE was calibrated using ammonium sulfate a few times during the campaign, and the average value of 0.9 ± 0.1 was applied to the entire campaign. The collection efficiency (CE) was determined as 1.0 for IOP1 according to volume comparison to the two co-located Scanning Mobility Particle Sizers (Figure S6). Volume of black carbon (BC) accounted for 8 ± 6 % of the total volume measured by SMPS, for an assumed density of 1.8 g cm^{-3} for BC. Since BC data were limited, the abscissa of Figure S6 was not subtracted by BC contribution. This CE value was consistent with that used for the AMAZE-08 in the wet season of 2008 (Chen et al., 2009).

S1.2 Semi-Volatile Thermal desorption Aerosol Gas Chromatography: set up and operation

Online measurements of organic tracer compounds in the particle and gas phases were made by a Semi-Volatile Thermal desorption Aerosol Gas chromatograph (SV-TAG). This instrument is described in detail elsewhere (Isaacman et al., 2014). Its operation is briefly presented here.

Air was sampled at 20 L min^{-1} from the center stream of a flow of 200 L min^{-1} through a 15.24 cm (OD) stainless steel duct at a height of approximately 5 m above ground level. The flow was then divided into two channels, passing through a PM1 cyclone at 10 L min^{-1}, each containing a custom Filter Collection and Thermal Desorption cell (F-CTD). The F-CTD quantitatively collected and retained both particle- and gas-phase compounds. A multi-channel carbon denuder (MAST Carbon) was used to remove all gases upstream of one collection cell. In this way, two samples were simultaneously collected: a "particle" sample and a "total" gas-plus-particle sample. Samples were thermally desorbed from the cells subjected to a ramping temperature from 30 to 310 °C (35 °C min^{-1}) into a helium stream that was 80% saturated with

MSTFA (N-Methyl-N-(trimethylsilyl) trifluoroacetamide). Hydroxyl groups were converted into silyl esters and ethers. Analytes were transferred to the GC column, and the sample was analyzed through a commercially available GC/MS (7890A/5975C; Agilent Technologies). The chromatographic data were analyzed using the publicly available software *TAG ExploreR and iNtegration* (Isaacman-VanWertz and Sueper).

Compounds were quantified using isotopically labeled internal standards to correct for run-to-run variability in sample transfer efficiency and instrument response. Regular multi-point calibrations were made of approximately 100 authentic standards. Pentaerythritol-2-^{13}C was used for 2-methyltetrols and C_5-alkene triols. The uncertainty in mass concentration was approximately 15% (Isaacman et al., 2014). C_5-alkene triols were quantified using the calibration factor of 2-methyltetrols under the assumption of an identical total ion response. An absence of an authentic standard results in unconstrained uncertainty in mass concentration of 30 of 50% (Jaoui et al., 2005).

S1.3 NO_y measurements

The NO_y measured included the following species: NO, NO_2, HNO_3, particle nitrate, RNO_3, and PAN. Measurements were made by a custom analyzer designed by Air Quality Design (AQD; http://www.airqualitydesign.com). The analyzer was based on two commercial oxides of nitrogen detectors made by Thermo Scientific (Model 42i TLE) and extensively modified by AQD. An external, temperature-controlled inlet box was mounted at 10 m above ground level.

The instrument contained both a research grade LED photolysis cell for converting NO_2 into NO and a heated molybdenum converter for converting total NO_y into NO. One channel, leading from the photolysis cell to one 42i TLE detector, alternated every minute between NO

and NO_x by switching the LED photoloysis cell on/off. The other channel, leading from the molybdenum converter to the second 42i TLE detector, measured total NO_y. The detectors internally measured zero based on pre-reaction of the sample with ozone. Instrument response was measured by addition of NO in zero air at the sampling point (10 m). Converter efficiency was measured by gas-phase titration of the NO standard to NO_2. An HNO_3 source was sampled every other day. The calibration unit was a Thermo Scientific Model 146i calibrator equipped with gas-phase titration and a permeation oven. The raw NO_y measurements, reported at a resolution of 10 s, were averaged into bins of 30 min to filter for local events not representative of the larger scale chemical processes that form the scope of this study.

S2. Positive Matrix Factorization and the IEPOX-SOA factor

The time series of mass spectra of organic material measured by the AMS was analyzed by positive matrix factorization (PMF) using a standard analysis toolkit (Ulbrich et al., 2009). High-resolution, V-mode data were used. The PMF solution was based on minimization of the "Q-value" or "PMF quality-of fit parameter", meaning the sum of the weighed squared residuals for a chosen number of factors. The interpretation of the physical significance of the AMS PMF factors took into account correlations with quantities simultaneously measured by other instruments. The solution consisted of six factors, and the present study focuses on one of the derived factors, labeled "IEPOX-SOA". de Sá (in preparation) focuses on presentation of the other factors.

The profile of the resolved IEPOX-SOA factor is shown in Figure S1. A key characteristic is intensity at $C_5H_6O^+$ (*m/z* 82) (Hu et al., 2015). In addition, a prominent signal at $C_4H_5^+$ (*m/z* 53) is observed, which has also been reported as characteristic of the IEPOX-SOA factor (Hu et al., 2015). The IEPOX-SOA factor is also relatively highly oxidized, as expressed

by f_{44} = 0.15 and oxygen to carbon atomic ratio O:C = 0.80, applying the calibration described in Canagaratna et al. (2015).

Technical diagnostics of the six-factor solution are presented in Figure S2 and more extensively described in (de Sá, in preparation). Panel b shows the quality of fit parameter $Q/Q_{expected}$ (Ulbrich et al., 2009) as a function of the number of factors, suggesting that the solution should have at least three factors. Panel a shows a great reduction in the structure of the total residuals when going from the five-factor to the six-factor solution. The six-factor solution also offered more meaningful factor profiles ("mass spectra") (de Sá, in preparation). Panel c shows $Q/Q_{expected}$ as a function of the rotational ambiguity parameter f_{peak} (Ulbrich et al., 2009) for the six-factor solution. A plausible range for f_{peak} was determined according to the best practice of limiting $Q/Q_{expected}$ to a value that does not exceed 0.1% of the minimum value (occurring at f_{peak} = 0). The default value of f_{peak} = 0 was chosen for the final six-factor solution, since no significant improvements in the external validation of the factors were observed. Moreover, the IEPOX-SOA factor resolved in the six-factor solution had a very robust time trend across a range of rotations in the solution (Figure S2d). As f_{peak} varied, the correlation of factor loading with C5-alkene triols concentrations remained approximately constant, even as some features of the factor profile changed significantly, such as the relative signals of $C_5H_6O^+$ and CO_2^+, respectively $f(C_5H_6O)$ and $f(CO_2)$, as well as the magnitude of factor loadings and consequently the ratio f.

The loading of the IEPOX-SOA factor may be an overestimate or an underestimate of the atmospheric concentration of the IEPOX-derived PM (brown dashed lines in Figure 1). In respect to overestimate, the AMS mass spectrum observed in laboratory studies for the uptake of IEPOX by acidic sulfate particles is statistically equal to that obtained for the uptake of isoprene

139 photo-oxidation products, yet IEPOX accounted for only half of those products (Liu et al., 2015).
140 The implication is that the uptake of non-IEPOX species can lead to a similar AMS spectrum.
141 Pathways of PM production from condensation of multifunctional hydroperoxides lead to a
142 distinct mass spectrum from IEPOX pathways, and are not expected to be highly active under the
143 acidic particle conditions of these experiments (Riva et al., 2016), leaving a large mass fraction
144 of produced PM unexplained. The combination of AMS vaporization at 600 °C and ionization by
145 electron impact at 70 eV may convert IEPOX-derived and non-IEPOX-derived molecules into
146 similar groups of ions, which then give rise to a similar mass spectrum. The SV-TAG, which
147 uses desorption temperatures up to 310 °C and thus can also induce thermal decomposition of
148 some molecules, might also result in an in-common analyte (i.e., tracer) between IEPOX-derived
149 and non-IEPOX-derived molecules, thereby precluding a constraint on any possible overestimate
150 by the AMS factor (Isaacman-VanWertz et al., 2016; Lopez-Hilfiker et al., 2016). For these
151 reasons, the loading of the IEPOX-SOA factor might overestimate IEPOX-derived PM
152 concentrations by accounting for other isoprene oxidation products that are not produced through
153 the IEPOX intermediate.

154 In respect to underestimate, the loading of the IEPOX-SOA factor may not capture the
155 entire particle-phase carbon footprint that originated from IEPOX uptake. Extensive atmospheric
156 processing, such as reactions with hydroxyl radicals or photolysis, can partly eliminate the initial
157 products of IEPOX uptake (Kroll et al., 2009; Bateman et al., 2011; Epstein et al., 2014; Hu et
158 al., 2015; Hu et al., 2016). The IEPOX-originated carbon can still be inside the particle, yet it no
159 longer contributes to the loading of the IEPOX-SOA factor because of an altered mass spectrum
160 for some molecules. Atmospheric reactions gradually homogenize particle composition and
161 properties, and the AMS spectra can become more uniform (Jimenez et al., 2009). Specifically,

the ratio of signal intensity at *m*/*z* 44 to that at *m*/*z* 43 increases, and the relative intensity of *m*/*z* 82 decreases (Ng et al., 2011; Hu et al., 2015). This modified organic material, which originally entered the particle phase through IEPOX uptake, may then contribute to the loading of PMF factors other than IEPOX-SOA, such as the oxidized organic factors broadly labeled as "OOA" (Zhang et al., 2005). For these several reasons, the IEPOX-SOA factor loading might be an underestimate of IEPOX-derived PM concentrations.

S3. Comparison of background and polluted cases

The presence of a pollution plume at T3 is indicated by a combination of several external measured variables, including particle number, ozone, and NO_y concentrations. The definition of background and polluted cases aimed at selecting afternoons that were associated with extreme values of those variables. Conditions entailing concentration of ozone at around 10 ppb or less, particle number concentration of less than 500 cm^{-3}, and NO_y concentrations of less than 1 ppb were collectively a strong indicative of a background case. Conditions including ozone concentrations upward of 30 ppb, particle number concentration above 2000 cm^{-3}, and NO_y concentrations around 1.5 ppb or above indicated pollution. Measurements of these variables onboard the G-1 aircraft confirmed what the ground measurements suggested on the several days that the G-1 flew overhead.

Examples of these supporting data are illustrated in Figure 3 for the chosen background and polluted days (March 3 and 13, 2014, respectively) composing the primary case study analyzed in the main text. A few other afternoons, representative of these two extremes of background and polluted cases, were selected from the campaign time series and are depicted in Figure S4. The top panel shows cases of background conditions, and the bottom panel shows cases of polluted conditions. The local wind direction observed for the polluted cases generally

characterized by easterlies, as consistent with Manaus direction, whereas for the background cases it tends to diverge from that prevailing direction. The cases within each category are ordered from left to right in ascending order of IEPOX-SOA factor loadings.

Sulfate concentrations had a wide range of values, even for background conditions (Figure S4), as discussed in the main text. Meteorological conditions such as overcast (lower photoxidation activity) and rain events (higher wet deposition), as seen on March 20 and March 23, are some of the factors that control particle number and mass concentration (sulfate and organic compounds). These factors help to explain the natural variability in sulfate mass concentration. By comparison, on a sunny day, with winds mostly coming from the northeast direction, as exemplified by February 16 and March 3, sulfate mass concentrations can be around 0.3 $\mu g\ m^{-3}$ or more, values which are also typical of some polluted days (bottom panel). Both the factor loading and the ratio f increased with increasing sulfate (rows 2 and 3 of top panel), when NO_y levels were approximately the same. A comparison of February 16 and March 3 shows in addition the importance of NO_y concentration: for similar concentrations of sulfate and organic PM and similar meteorological conditions, the case having lower NO_y concentrations (0.4 to 0.5 ppb on March 3 as compared to 0.7 to 0.8 ppb on February 16) was associated with considerably higher absolute and relative factor loadings.

For the polluted cases shown in Figure S4, NO_y concentrations were variable between and within cases, ranging from 1 ppb up to 7 ppb. Larger sulfate mass concentrations (from left to right) were associated with larger absolute and relative factor loadings, analogous to what was observed for background cases. A comparison between March 3 and 13 (i.e., background and polluted; Figure 4) shows that for similar sulfate concentrations but higher NO_y levels March 13 had considerably lower factor loadings. The case of February 9 (polluted) illustrates that the

208 factor loadings did not exceed 0.4 μg m^{-3} and *f* did not exceed 0.2 even at rarely high sulfate
209 concentrations in the wet season, reaching 0.9 μg m^{-3}. This finding is attributed to the high NO
210 concentrations, as implied by NO_y concentrations of 3 ppb and greater, that suppressed IEPOX
211 production.

212 These cases illustrate the possible wide range of observed sulfate mass concentrations
213 under background conditions, in great part overlapping with typical values of polluted
214 conditions. The cases also demonstrate that the trend in observed IEPOX-SOA factor loadings
215 and ratio *f*, both within each category (background or polluted conditions) and between them, can
216 be consistently explained by the roles that sulfate and NO exert on the production of IEPOX-
217 derived PM.

218 **S4. Sulfate and particle acidity estimates in the context of field studies**

219 The underlying relative importance of direct compared to indirect roles of sulfate on the
220 formation of IEPOX-derived PM is not well understood. Sulfate can play a direct role as a
221 nucleophile in the reaction of formation of organosulfates from IEPOX (Surratt et al., 2007b;
222 Nguyen et al., 2014). Organosulfates, however, are believed to constitute only a fraction of the
223 IEPOX-derived PM (Hu et al., 2015). Particle acidity, an indirect effect of sulfate, has been
224 shown to drive IEPOX-derived PM production in several lab studies (Surratt et al., 2007a;
225 Kuwata et al., 2015; Lewandowski et al., 2015). Nevertheless, the acidity effect observed in
226 laboratories is not as clearly observed in field studies, wherein pH estimates have typically been
227 employed as a proxy for acidity (Budisulistiorini et al., 2013; Lin et al., 2013; Worton et al.,
228 2013; Budisulistiorini et al., 2015; Xu et al., 2015). The present study corroborates those findings
229 and further argues that this apparent conflict can be reasoned by taking into account that both the
230 estimate and the end-use of pH may be problematic in the context of field studies.

231 Firstly, a reliable estimate of pH is often hard to obtain. In the case of the present study,
232 some difficulties were imposed by data availability. Gas-phase measurements of NH_3 or HNO_3
233 were not available for performing "forward" mode calculations in thermodynamic models or gas-
234 particle phase partitioning calculations, which have been suggested as the best method to predict
235 pH (Hennigan et al., 2015). Co-located independent measurements of ion concentrations (e.g., by
236 chromatograph) were not available to confirm the ion balance obtained by AMS measurements
237 (Figure S7).
238 Bearing these caveats in mind, the analysis presented in the main text using sulfate as a
239 predictor for IEPOX-SOA was replicated here using pH in place of sulfate. Figure S8 is
240 analogous to Figure 6a. pH was estimated for IOP1 using AMS measurements of mass
241 concentrations of inorganic ions (sulfate, ammonium, nitrate, and chloride) and measurements of
242 RH and temperature. The E-AIM model II (Clegg et al., 1998) was employed. The final pH was
243 calculated taking into account both the inorganic water predicted by the model and the organic
244 water estimated from organic hygroscopicity κ_{org} values (Thalman, in preparation), in a similar
245 fashion as described by Guo et al. (2015). Figure S8 shows that pH, as calculated herein and for
246 the caveats herein, does not work well as a predictor for IEPOX-SOA factor loading. Figure S9
247 is analogous to Figure 7. Figure S9 shows that, although the overall dependencies on NO_y are
248 similar to analysis of the data by sulfate, the separation by pH yields groups that have less
249 distinct trends and ranges among them.
250 In addition to difficulties associated with generating accurate estimates of pH, there is an
251 inconsistency between the timescales of estimated particle acidity and IEPOX-SOA factor
252 loadings that may preclude underlying correlations to emerge. The estimated pH makes use of
253 instantaneous RH and temperature values and is therefore an instantaneous estimate of pH. They

can change in timescales of 15 min or less giving mixing in the boundary layer, for example. On the other hand, sulfate mass concentrations and IEPOX-SOA factor loadings are variables representative of processes of longer time scales of hours and days. By not containing any information on the particle acidity history in the past hours or days, the calculated instantaneous pH may fail in capturing the true effect of acidity on the chemical formation of IEPOX-derived PM. The RH cycling history of sulfate particles has been demonstrated to mediate the extent of IEPOX-derived PM production (Wong et al., 2015). Moreover, sulfate, by being intrinsically related to particle acidity and at the same time a species of congruent lifetime with secondary organic material, may in fact be a better proxy to capture the history of particle acidity than estimates of pH. For these different reasons, sulfate rather than pH is used in the analysis herein. The understanding, however, is that sulfate represents effects beyond those of the direct chemical role of sulfate. In analogy to pH, this discussion also extends to the use of sulfate rather than instantaneous particle water content as the predictor of IEPOX-SOA factor loadings.

S5. Five subsets of data based on NO_y concentrations

The data subsets and fits shown in Figure 6 are shown in separate panels in Figure S5. Once a trend of decreasing fit slope with increasing NO_y concentration was identified, the number of data subsets was defined as the minimum necessary to have subsets of at least 100 data points (of a total of 888) to allow for robust statistics and that were also cohesive (as measured by R^2) and non-redundant (i.e., of different fit lines).

The coloring by date in Figure S5 shows that there is no apparent correlation between levels of NO_y concentration or goodness of fit with different time periods within IOP1. Meteorological variables such as solar radiation, temperature, and RH (not shown) are also not able to delineate any clear pattern in the data, either within or among groups.

Although a linear bivariate statistical analysis for the IEPOX-SOA factor in sulfate and NO_y concentrations at first appears attractive, the underlying chemical processes were not linear, as reflected in the relationship between IEPOX-derived PM and NO_y concentrations. Moreover, sulfate and NO_y concentrations were not independent variables. For these reasons, a linear bivariate analysis is not appropriate, and a subset analysis was pursued instead.

S6. Details and assumptions of the model

The solution to the differential Equation 1 is as follows:

$$M(t) = \frac{\alpha_P k_P}{\alpha_L k_L} + e^{\alpha_L k_L t}\left(M_0 - \frac{\alpha_P k_P}{\alpha_L k_L}\right) \quad \text{(S1)}$$

for which the subscript 0 indicates initial (background) conditions, i.e., immediately before the airmass passes over Manaus. For the transport from Manaus to T3, $t = \tau_{tr}$, and the variable M represents the IEPOX-derived PM mass concentrations at T3.

The zero-order production rate coefficient k_P and the first-order loss rate coefficient k_L are lumped parameters representative of several production and loss processes, respectively. A first assumption is that they are constant over the course of four hours. In hand with that assumption, a constant boundary layer height throughout the integration time is assumed. The τ values represent the time required under afternoon conditions to significantly affect the IEPOX-derived PM mass concentration by the corresponding processes. For afternoon time periods, observations show that $dM/dt > 0$ over tropical forests in the absence of pollution (Chen et al., 2009; Chen et al., 2015).The parameter τ_P, corresponding to a first order process, therefore represents an instantaneous quantity in the transient system. For simplicity of presentation, τ_P is defined in reference to M_0, although defining it in relation to M_{bg} or M_{pol} does not alter the main conclusions presented herein.

In terms of loss processes, represented by the rate coefficient k_L, IEPOX-derived PM may be lost by three main mechanisms: heterogeneous oxidation against OH, condensed-phase reactions, and dry deposition. The lifetime of IEPOX-derived PM against heterogeneous oxidation is estimated at around two weeks for an OH concentration of 10^6 molecules cm^{-3} (Hu et al., 2016). Lifetime of IEPOX products against particle-phase reactions has not yet been reported but is expected to be at least several days. A value of one week is used here. The lifetime of PM against deposition is on the order of a week. The overall loss process is then approximated in the model as the sum of these three processes, which leads to an estimate of overall loss rate coefficient $k_L = 0.015\ h^{-1}$ (overall characteristic time of 2.8 days).

In respect to wet deposition along the track from Manaus to the T3 site, strong convection imports background regional air, and for this reason strong wet deposition is mathematically equivalent in the model developed herein to a trajectory that does not pass over Manaus, i.e., background conditions. Weak wet deposition represents a mixing of polluted and background air masses, giving rise to intermediate NO_y concentrations. Entrainment on the plume edges as well as with the free troposphere is mathematically similar to wet deposition in the model framework. Thus entrainment and wet deposition, without directly contributing to k_L, are indirectly incorporated in the developed model based on their effects on NO_y concentration.

In terms of production processes, represented by the rate coefficient k_P, IEPOX-derived PM is produced by multigenerational chemistry of isoprene photooxidation and reactive uptake. Model Case 1 investigated the sensitivity of pollution enhancement ratio and absolute mass concentration of IEPOX-derived PM to its production rate coefficient. After constrained by observations, the estimated interval for k_P was [0.07, 0.13] $\mu g\ m^{-3}\ h^{-1}$. In addition, values of $k_P >$ 0.2 $\mu g\ m^{-3}\ h^{-1}$ are unlikely given the rare observation (<1%) of $M_{bg} > 1 \mu g\ m^{-3}$.

The obtained range can be compared to estimates of total production rate of organic material from diameter growth rates. Firstly, a relative production rate of 1:3 for IEPOX-derived PM to total organic PM is assumed based on the following. IEPOX-derived PM is estimated to contribute 34% on average to total organic PM in central Amazonia under background conditions (Chen et al., 2015). For assumptions of equal first order loss rate coefficients for all organic material, a mass concentration ratio of 1:3 for IEPOX-derived PM to total organic material implies a ratio of 1:3 in their production rate coefficients k_P. As a consequence, the estimated range for total organic material is [0.21, 0.39] μg m^{-3} h^{-1}. For the estimate of organic material production based on growth rates, an average growth rate of 10 nm h^{-1} (Kulmala et al., 2004) is assumed. Further assumptions are a range of particle number concentration of 500 to 1000 cm^{-3} and of initial diameter of 20 to 100 nm, typical of background conditions in the Amazon. The obtained range of organic material production from growth rate estimates is therefore 0.02 to 0.32 μg m^{-3} h^{-1}, which is comparable to the range constrained by the model.

In terms of the influence of Manaus plume on the production and loss processes, the following assumptions were made. The acceleration of the oxidant cycle in the plume implies that $\alpha_L > 1$. Under plume conditions, OH concentrations observed at the T3 site increased by a factor of three compared to background conditions (Martin et al., 2017; Kim, in preparation). A proportional increase in the loss rate of IEPOX-derived PM by OH heterogeneous chemistry in the plume is expected. While the OH loss mechanism (of characteristic time of two weeks) is accelerated by three fold in the plume, dry deposition and condensed phase reactions (both of assumed characteristic times of a week) are held constant. As a result, the overall loss rate is enhanced by two fold, i.e., $\alpha_L = 2$ is assumed.

Concerning the production enhancement factor, the interception of ISOPOO radicals by NO in the pollution plume as well as the faster consumption of intermediate gas-phase species by the enhanced OH and O_3 concentrations implies $\alpha_P < 1$. The assumption is that the production of IEPOX almost halts in the plume, and $\alpha_P = 0.1$. This assumption is supported by measured gas-phase concentrations of ISOPOOH at the T3 site, which dropped by 90% when NO_y concentrations increased from 0.5 ppb to 2 ppb (Liu et al., 2016). This observation and the associated model assumption are a reflection of the lifetimes of the chemical species discussed: in contrast to the abovementioned lifetimes on order of a week for organic particle material against loss processes, the lifetimes of the gaseous species are significantly shorter. Isoprene and ISOPOOH have a lifetime on the order of a few hours (Eddingsaas et al., 2010; St. Clair et al., 2015), and IEPOX has a lifetime of a few hours to a day for an OH concentration of 10^6 molecules cm^{-3} (Jacobs et al., 2013; Bates et al., 2014).

Supplementary References

Bateman, A. P., Nizkorodov, S. A., Laskin, J., and Laskin, A.: Photolytic processing of secondary organic aerosols dissolved in cloud droplets, Phys. Chem. Chem. Phys., 13, 12199-12212, 2011, 10.1039/C1CP20526A.

Bates, K. H., Crounse, J. D., St. Clair, J. M., Bennett, N. B., Nguyen, T. B., Seinfeld, J. H., Stoltz, B. M., and Wennberg, P. O.: Gas phase production and loss of isoprene epoxydiols, J. Phys. Chem. A, 118, 1237-1246, 2014, 10.1021/jp4107958.

Budisulistiorini, S. H., Canagaratna, M. R., Croteau, P. L., Marth, W. J., Baumann, K., Edgerton, E. S., Shaw, S. L., Knipping, E. M., Worsnop, D. R., Jayne, J. T., Gold, A., and Surratt, J. D.: Real-time continuous characterization of secondary organic aerosol derived from isoprene epoxydiols in downtown Atlanta, Georgia, using the Aerodyne Aerosol Chemical Speciation Monitor, Environ. Sci. Technol., 47, 5686-5694, 2013, 10.1021/es400023n.

Budisulistiorini, S. H., Li, X., Bairai, S. T., Renfro, J., Liu, Y., Liu, Y. J., McKinney, K. A., Martin, S. T., McNeill, V. F., Pye, H. O. T., Nenes, A., Neff, M. E., Stone, E. A., Mueller, S., Knote, C., Shaw, S. L., Zhang, Z., Gold, A., and Surratt, J. D.: Examining the effects of anthropogenic emissions on isoprene-derived secondary organic aerosol formation during the 2013 Southern Oxidant and Aerosol Study (SOAS) at the Look Rock, Tennessee ground site, Atmos. Chem. Phys., 15, 8871-8888, 2015, 10.5194/acp-15-8871-2015.

Canagaratna, M. R., Jayne, J. T., Jimenez, J. L., Allan, J. D., Alfarra, M. R., Zhang, Q., Onasch, T. B., Drewnick, F., Coe, H., Middlebrook, A., Delia, A., Williams, L. R., Trimborn, A. M., Northway, M. J., DeCarlo, P. F., Kolb, C. E., Davidovits, P., and Worsnop, D. R.: Chemical and microphysical characterization of ambient aerosols with the aerodyne

aerosol mass spectrometer, Mass Spectrom. Rev., 26, 185-222, 2007, 10.1002/mas.20115.

Canagaratna, M. R., Jimenez, J. L., Kroll, J. H., Chen, Q., Kessler, S. H., Massoli, P., Hildebrandt Ruiz, L., Fortner, E., Williams, L. R., Wilson, K. R., Surratt, J. D., Donahue, N. M., Jayne, J. T., and Worsnop, D. R.: Elemental ratio measurements of organic compounds using aerosol mass spectrometry: characterization, improved calibration, and implications, Atmos. Chem. Phys., 15, 253-272, 2015, 10.5194/acp-15-253-2015.

Chen, Q., Farmer, D. K., Schneider, J., Zorn, S. R., Heald, C. L., Karl, T. G., Guenther, A., Allan, J. D., Robinson, N., Coe, H., Kimmel, J. R., Pauliquevis, T., Borrmann, S., Pöschl, U., Andreae, M. O., Artaxo, P., Jimenez, J. L., and Martin, S. T.: Mass spectral characterization of submicron biogenic organic particles in the Amazon Basin, Geophys. Res. Lett., 36, L20806, 2009, 10.1029/2009GL039880.

Chen, Q., Farmer, D. K., Rizzo, L. V., Pauliquevis, T., Kuwata, M., Karl, T. G., Guenther, A., Allan, J. D., Coe, H., Andreae, M. O., Pöschl, U., Jimenez, J. L., Artaxo, P., and Martin, S. T.: Submicron particle mass concentrations and sources in the Amazonian wet season (AMAZE-08), Atmos. Chem. Phys., 15, 3687-3701, 2015, 10.5194/acp-15-3687-2015.

Clegg, S. L., Brimblecombe, P., and Wexler, A. S.: Thermodynamic model of the system H^+-NH_4^+-SO_4^{2-}-NO_3^--H_2O at tropospheric temperatures, J. Phys. Chem. A, 102, 2137-2154, 1998, 10.1021/jp973042r.

de Sá, S. S.: Anthropogenic emissions affect the sources and composition of submicron particulate matter in central Amazonia in the wet season, in preparation.

DeCarlo, P. F., Kimmel, J. R., Trimborn, A., Northway, M. J., Jayne, J. T., Aiken, A. C., Gonin, M., Fuhrer, K., Horvath, T., Docherty, K. S., Worsnop, D. R., and Jimenez, J. L.: Field-

deployable, high-resolution, time-of-flight aerosol mass spectrometer, Anal. Chem., 78, 8281-8289, 2006, 10.1021/ac061249n.

Eddingsaas, N. C., VanderVelde, D. G., and Wennberg, P. O.: Kinetics and products of the acid-catalyzed ring-opening of atmospherically relevant butyl epoxy alcohols, J. Phys. Chem. A, 114, 8106-8113, 2010, 10.1021/jp103907c.

Epstein, S. A., Blair, S. L., and Nizkorodov, S. A.: Direct photolysis of α-pinene ozonolysis secondary organic aerosol: effect on particle mass and peroxide content, Environ. Sci. Technol., 48, 11251-11258, 2014, 10.1021/es502350u.

Guo, H., Xu, L., Bougiatioti, A., Cerully, K. M., Capps, S. L., Hite Jr, J. R., Carlton, A. G., Lee, S. H., Bergin, M. H., Ng, N. L., Nenes, A., and Weber, R. J.: Fine-particle water and pH in the southeastern United States, Atmos. Chem. Phys, 15, 5211-5228, 2015, 10.5194/acp-15-5211-2015

Hu, W. W., Campuzano-Jost, P., Palm, B. B., Day, D. A., Ortega, A. M., Hayes, P. L., Krechmer, J. E., Chen, Q., Kuwata, M., Liu, Y. J., de Sá, S. S., McKinney, K., Martin, S. T., Hu, M., Budisulistiorini, S. H., Riva, M., Surratt, J. D., St. Clair, J. M., Isaacman-Van Wertz, G., Yee, L. D., Goldstein, A. H., Carbone, S., Brito, J., Artaxo, P., de Gouw, J. A., Koss, A., Wisthaler, A., Mikoviny, T., Karl, T., Kaser, L., Jud, W., Hansel, A., Docherty, K. S., Alexander, M. L., Robinson, N. H., Coe, H., Allan, J. D., Canagaratna, M. R., Paulot, F., and Jimenez, J. L.: Characterization of a real-time tracer for isoprene epoxydiols-derived secondary organic aerosol (IEPOX-SOA) from aerosol mass spectrometer measurements, Atmos. Chem. Phys., 15, 11807-11833, 2015, 10.5194/acp-15-11807-2015.

Hu, W. W., Palm, B., Day, D., Campuzano-Jost, P., Krechmer, J., Peng, Z., De Sá, S. S., Martin, S. T., Alexander, M. L., Baumann, K., Hacker, L., Kiendler-Scharr, A., Koss, A., De Gouw, J., Goldstein, A. H., Seco, R., Sjostedt, S., Park, J.-H., Guenther, A., Kim, S., Canonaco, F., Prevot, A., Brune, W., and Jimenez, J. L.: Long lifetime of ambient isoprene epoxydiols-derived Secondary Organic Aerosol (IEPOX-SOA) against OH oxidation and evaporation, Atmos. Chem. Phys. Disc., 2016, doi: 10.5194/acp-2016-418.

Isaacman-VanWertz, G. and Sueper, D.: TERN: TAG ExploreR and iNtegration https://sites.google.com/site/terninigor/.

Isaacman-VanWertz, G., Yee, L. D., Kreisberg, N. M., Wernis, R., Moss, J. A., Hering, S. V., de Sá, S. S., Martin, S. T., Alexander, M. L., Palm, B. B., Hu, W., Campuzano-Jost, P., Day, D. A., Jimenez, J. L., Riva, M., Surratt, J. D., Viegas, J., Manzi, A., Edgerton, E., Baumann, K., Souza, R., Artaxo, P., and Goldstein, A. H.: Ambient Gas-Particle Partitioning of Tracers for Biogenic Oxidation, Env. Sci. Technol., 2016, 10.1021/acs.est.6b01674.

Isaacman, G., Kreisberg, N., Yee, L., Worton, D., Chan, A., Moss, J., Hering, S., and Goldstein, A.: Online derivatization for hourly measurements of gas-and particle-phase semi-volatile oxygenated organic compounds by thermal desorption aerosol gas chromatography (SV-TAG), Atmos. Meas. Tech., 7, 4417-4429, 2014, 10.5194/amt-7-4417-2014.

Jacobs, M. I., Darer, A. I., and Elrod, M. J.: Rate constants and products of the OH reaction with isoprene-derived epoxides, Environ. Sci. Technol., 47, 12868-12876, 2013, 10.1021/es403340g.

Jaoui, M., Kleindienst, T., Lewandowski, M., Offenberg, J., and Edney, E.: Identification and quantification of aerosol polar oxygenated compounds bearing carboxylic or hydroxyl

groups. 2. Organic tracer compounds from monoterpenes, Environ. Sci. Technol., 39, 5661-5673, 2005, 10.1021/es048111b.

Jimenez, J. L., Canagaratna, M. R., Donahue, N. M., Prevot, A. S. H., Zhang, Q., Kroll, J. H., DeCarlo, P. F., Allan, J. D., Coe, H., Ng, N. L., Aiken, A. C., Docherty, K. S., Ulbrich, I. M., Grieshop, A. P., Robinson, A. L., Duplissy, J., Smith, J. D., Wilson, K. R., Lanz, V. A., Hueglin, C., Sun, Y. L., Tian, J., Laaksonen, A., Raatikainen, T., Rautiainen, J., Vaattovaara, P., Ehn, M., Kulmala, M., Tomlinson, J. M., Collins, D. R., Cubison, M. J., Dunlea, J., Huffman, J. A., Onasch, T. B., Alfarra, M. R., Williams, P. I., Bower, K., Kondo, Y., Schneider, J., Drewnick, F., Borrmann, S., Weimer, S., Demerjian, K., Salcedo, D., Cottrell, L., Griffin, R., Takami, A., Miyoshi, T., Hatakeyama, S., Shimono, A., Sun, J. Y., Zhang, Y. M., Dzepina, K., Kimmel, J. R., Sueper, D., Jayne, J. T., Herndon, S. C., Trimborn, A. M., Williams, L. R., Wood, E. C., Middlebrook, A. M., Kolb, C. E., Baltensperger, U., and Worsnop, D. R.: Evolution of organic aerosols in the atmosphere, Science, 326, 1525-1529, 2009, 10.1126/science.1180353.

Kim, S., in preparation.

Kroll, J. H., Smith, J. D., Che, D. L., Kessler, S. H., Worsnop, D. R., and Wilson, K. R.: Measurement of fragmentation and functionalization pathways in the heterogeneous oxidation of oxidized organic aerosol, Phys. Chem. Chem. Phys., 11, 8005-8014, 2009, 10.1039/B905289E.

Kulmala, M., Vehkamäki, H., Petäjä, T., Dal Maso, M., Lauri, A., Kerminen, V. M., Birmili, W., and McMurry, P. H.: Formation and growth rates of ultrafine atmospheric particles: a review of observations, J. Aerosol Sci., 35, 143-176, 2004, http://dx.doi.org/10.1016/j.jaerosci.2003.10.003.

Kuwata, M., Zorn, S. R., and Martin, S. T.: Using elemental ratios to predict the density of organic material composed of carbon, hydrogen, and oxygen, Environ. Sci. Technol., 46, 787-794, 2011, 10.1021/es202525q.

Kuwata, M., Liu, Y., McKinney, K., and Martin, S. T.: Physical state and acidity of inorganic sulfate can regulate the production of secondary organic material from isoprene photooxidation products, Phys. Chem. Chem. Phys., 17, 5670-5678, 2015, 10.1039/C4CP04942J.

Lewandowski, M., Jaoui, M., Offenberg, J., Krug, J., and Kleindienst, T.: Atmospheric oxidation of isoprene and 1, 3-butadiene: influence of aerosol acidity and relative humidity on secondary organic aerosol, Atmos. Chem. Phys., 15, 3773-3783, 2015, 10.5194/acp-15-3773-2015.

Lin, Y.-H., Knipping, E., Edgerton, E., Shaw, S., and Surratt, J. D.: Investigating the influences of SO_2 and NH_3 levels on isoprene-derived secondary organic aerosol formation using conditional sampling approaches, Atmos. Chem. Phys., 13, 8457-8470, 2013, 10.5194/acp-13-8457-2013.

Liu, Y., Kuwata, M., Strick, B. F., Geiger, F. M., Thomson, R. J., McKinney, K. A., and Martin, S. T.: Uptake of epoxydiol isomers accounts for half of the particle-phase material produced from isoprene photooxidation via the HO_2 pathway, Environ. Sci. Technol., 49, 250-258, 2015, 10.1021/es5034298.

Liu, Y., Brito, J., Dorris, M. R., Rivera-Rios, J. C., Seco, R., Bates, K. H., Artaxo, P., Duvoisin, S., Keutsch, F. N., Kim, S., Goldstein, A. H., Guenther, A. B., Manzi, A. O., Souza, R. A. F., Springston, S. R., Watson, T. B., McKinney, K. A., and Martin, S. T.: Isoprene

photochemistry over the Amazon rain forest, Proc. Natl. Acad. Sci. USA, 113, 6125-6130, 2016, 10.1073/pnas.1524136113.

Lopez-Hilfiker, F. D., Mohr, C., D'Ambro, E. L., Lutz, A., Riedel, T. P., Gaston, C. J., Iyer, S., Zhang, Z., Gold, A., Surratt, J. D., Lee, B. H., Kurten, T., Hu, W. W., Jimenez, J., Hallquist, M., and Thornton, J. A.: Molecular composition and volatility of organic aerosol in the Southeastern US: implications for IEPOX derived SOA, Environ. Sci. Technol., 2200–2209, 2016, 10.1021/acs.est.5b04769.

Martin, S. T., Artaxo, P., Machado, L. A. T., Manzi, A. O., Souza, R. A. F., Schumacher, C., Wang, J., Andreae, M. O., Barbosa, H. M. J., Fan, J., Fisch, G., Goldstein, A. H., Guenther, A., Jimenez, J. L., Pöschl, U., Silva Dias, M. A., Smith, J. N., and Wendisch, M.: Introduction: observations and modeling of the green ocean Amazon (GoAmazon2014/5), Atmos. Chem. Phys., 16, 4785-4797, 2016, 10.5194/acp-16-4785-2016.

Martin, S. T., Artaxo, P., Machado, L., Manzi, A. O., Souza, R. A. F., Schumacher, C., Wang, J., Biscaro, T., Brito, J., Calheiros, A., Jardine, K., Medeiros, A., Portela, B., Sá, S. S. d., Adachi, K., Aiken, A. C., Albrecht, R., Alexander, L., Andreae, M. O., Barbosa, H. M. J., Buseck, P., Chand, D., Comstock, J. M., Day, D. A., Dubey, M., Fan, J., Fast, J., Fisch, G., Fortner, E., Giangrande, S., Gilles, M., Goldstein, A. H., Guenther, A., Hubbe, J., Jensen, M., Jimenez, J. L., Keutsch, F. N., Kim, S., Kuang, C., Laskin, A., McKinney, K., Mei, F., Miller, M., Nascimento, R., Pauliquevis, T., Pekour, M., Peres, J., Petäjä, T., Pöhlker, C., Pöschl, U., Rizzo, L., Schmid, B., Shilling, J. E., Dias, M. A. S., Smith, J. N., Tomlinson, J. M., Tóta, J., and Wendisch, M.: The Green ocean Amazon Experiment

(GoAmazon2014/5) observes pollution affecting gases, aerosols, clouds, and rainfall over the rain forest, B. Am. Meteorol. Soc., 2017, doi:10.1175/BAMS-D-15-00221.1.

Ng, N., Canagaratna, M., Jimenez, J., Chhabra, P., Seinfeld, J., and Worsnop, D.: Changes in organic aerosol composition with aging inferred from aerosol mass spectra, Atmos. Chem. Phys., 11, 6465-6474, 2011, 10.5194/acp-11-6465-2011.

Nguyen, T. B., Coggon, M. M., Bates, K. H., Zhang, X., Schwantes, R. H., Schilling, K. A., Loza, C. L., Flagan, R. C., Wennberg, P. O., and Seinfeld, J. H.: Organic aerosol formation from the reactive uptake of isoprene epoxydiols (IEPOX) onto non-acidified inorganic seeds, Atmos. Chem. Phys., 14, 3497-3510, 2014, 10.5194/acp-14-3497-2014.

Riva, M., Budisulistiorini, S. H., Chen, Y., Zhang, Z., D'Ambro, E. L., Zhang, X., Gold, A., Turpin, B. J., Thornton, J. A., Canagaratna, M. R., and Surratt, J. D.: Chemical characterization of secondary organic aerosol from oxidation of isoprene hydroxyhydroperoxides, Environ. Sci. Technol., 2016, 10.1021/acs.est.6b02511.

St. Clair, J. M., Rivera-Rios, J. C., Crounse, J. D., Knap, H. C., Bates, K. H., Teng, A. P., Jørgensen, S., Kjaergaard, H. G., Keutsch, F. N., and Wennberg, P. O.: Kinetics and products of the reaction of the first-generation isoprene hydroxy hydroperoxide (ISOPOOH) with OH, J. Phys. Chem. A, 2015, 10.1021/acs.jpca.5b06532.

Surratt, J. D., Lewandowski, M., Offenberg, J. H., Jaoui, M., Kleindienst, T. E., Edney, E. O., and Seinfeld, J. H.: Effect of acidity on secondary organic aerosol formation from isoprene, Environ. Sci. Technol., 41, 5363-5369, 2007a, 10.1021/es0704176.

Surratt, J. D., Kroll, J. H., Kleindienst, T. E., Edney, E. O., Claeys, M., Sorooshian, A., Ng, N. L., Offenberg, J. H., Lewandowski, M., Jaoui, M., Flagan, R. C., and Seinfeld, J. H.:

Evidence for organosulfates in secondary organic aerosol, Environ. Sci. Technol., 41, 517-527, 2007b, 10.1021/es062081q.

Thalman, R., in preparation.

Ulbrich, I., Canagaratna, M., Zhang, Q., Worsnop, D., and Jimenez, J.: Interpretation of organic components from Positive Matrix Factorization of aerosol mass spectrometric data, Atmos. Chem. Phys., 9, 2891-2918, 2009, 10.5194/acp-9-2891-2009.

Wong, J. P., Lee, A. K., and Abbatt, J. P.: Impacts of Sulfate Seed Acidity and Water Content on Isoprene Secondary Organic Aerosol Formation, Environ. Sci. Technol., 49, 13215-13221, 2015, 10.1021/acs.est.5b02686.

Worton, D. R., Surratt, J. D., LaFranchi, B. W., Chan, A. W. H., Zhao, Y., Weber, R. J., Park, J.-H., Gilman, J. B., de Gouw, J., Park, C., Schade, G., Beaver, M., Clair, J. M. S., Crounse, J., Wennberg, P., Wolfe, G. M., Harrold, S., Thornton, J. A., Farmer, D. K., Docherty, K. S., Cubison, M. J., Jimenez, J.-L., Frossard, A. A., Russell, L. M., Kristensen, K., Glasius, M., Mao, J., Ren, X., Brune, W., Browne, E. C., Pusede, S. E., Cohen, R. C., Seinfeld, J. H., and Goldstein, A. H.: Observational insights into aerosol formation from isoprene, Environ. Sci. Technol., 47, 11403-11413, 2013, 10.1021/es4011064.

Xu, L., Guo, H., Boyd, C. M., Klein, M., Bougiatioti, A., Cerully, K. M., Hite, J. R., Isaacman-VanWertz, G., Kreisberg, N. M., Knote, C., Olson, K., Koss, A., Goldstein, A. H., Hering, S. V., de Gouw, J., Baumann, K., Lee, S.-H., Nenes, A., Weber, R. J., and Ng, N. L.: Effects of anthropogenic emissions on aerosol formation from isoprene and monoterpenes in the southeastern United States, Proc. Natl. Acad. Sci. USA, 112, 37-42, 2015, 10.1073/pnas.1417609112.

Zhang, Q., Alfarra, M. R., Worsnop, D. R., Allan, J. D., Coe, H., Canagaratna, M. R., and Jimenez, J. L.: Deconvolution and quantification of hydrocarbon-like and oxygenated organic aerosols based on aerosol mass spectrometry, Environ. Sci. Technol., 39, 4938-4952, 2005, 10.1021/es048568l.

Zhang, X., Smith, K. A., Worsnop, D. R., Jimenez, J. L., Jayne, J. T., Kolb, C. E., Morris, J., and Davidovits, P.: Numerical characterization of particle beam collimation: part II integrated aerodynamic-lens–nozzle system, Aerosol Sci. Technol., 38, 619-638, 2004, 10.1080/02786820490479833.

List of Supplementary Figures

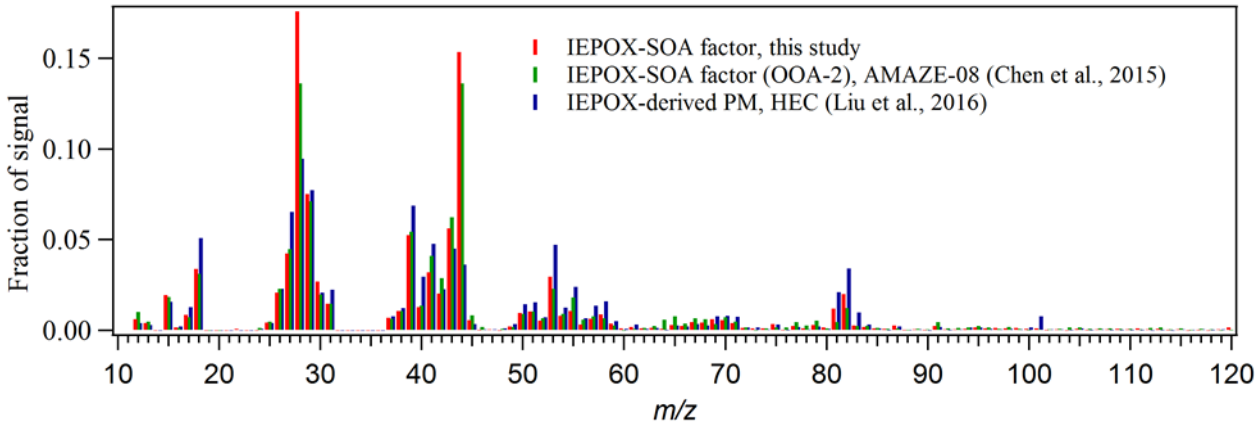

Figure S1. Profile of the IEPOX-SOA factor resolved by PMF analysis of the time series of AMS organic mass spectra collected in the wet season of 2014 (IOP1) at the T3 site (red), and in the wet season of 2008 (green) as part of AMAZE-08 experiment at the T0t site (Chen et al., 2015). Also plotted is the mass spectrum of secondary organic material produced in the Harvard Environmental Chamber from β-IEPOX photooxidation onto acidic ammonium sulfate seed particles under HO_2-dominant conditions and RH < 5% (blue) (Liu et al., 2015). Pearson correlation coefficients *R* between the PMF factor of this study and the other spectra were: R = 0.99 for the AMAZE-08 PMF factor, R = 0.81 for the chamber spectrum with all ions included, and R = 0.95 for the chamber spectrum with *m/z* 44 and 28 excluded.

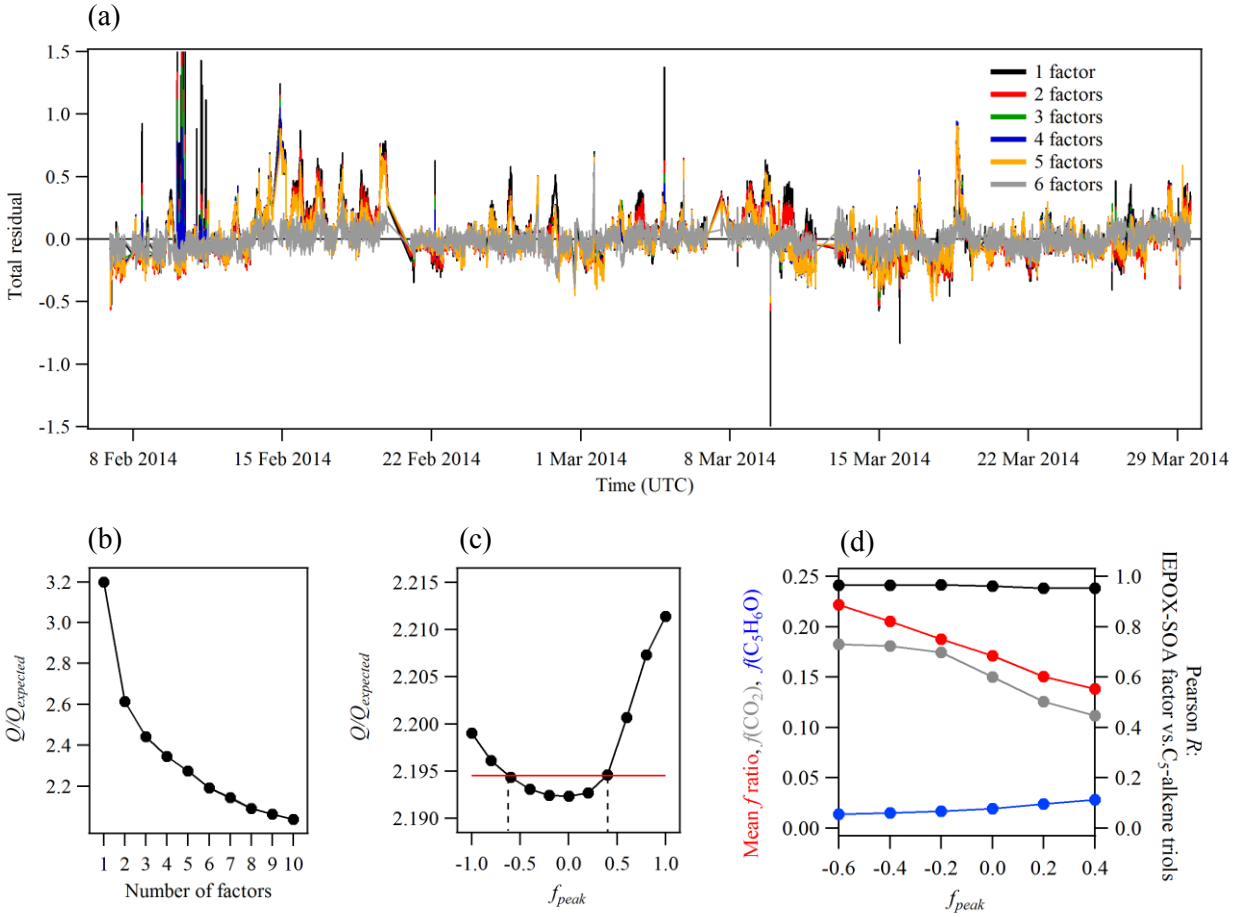

Figure S2. (a) Time series of total ion residuals of PMF solutions from one to six factors, (b) Dependence of the quality-of-fit parameter $Q/Q_{expected}$ on the number of factors for $f_{peak} = 0$, (c) Dependence of the quality-of-fit parameter $Q/Q_{expected}$ on f_{peak} for number of factors = 6. The red line represents $Q/Q_{expected}$ that exceeds in 0.1% the minimum value at $f_{peak} = 0$. This limit determines the range of plausible f_{peak} values as indicated by the dashed black lines, (d) For the six-factor solution, dependence on the f_{peak} parameter of the Pearson correlation coefficient R between the IEPOX-SOA factor loadings and independently measured C_5-alkene triols (on the right vertical axis), the mean f ratio of IEPOX-SOA factor loading to total organic PM mass concentration, and the relative intensities $f(CO_2)$ and $f(C_5H_6O)$of the ions CO_2^+ and $C_5H_6O^+$, respectively (on the left vertical axis).

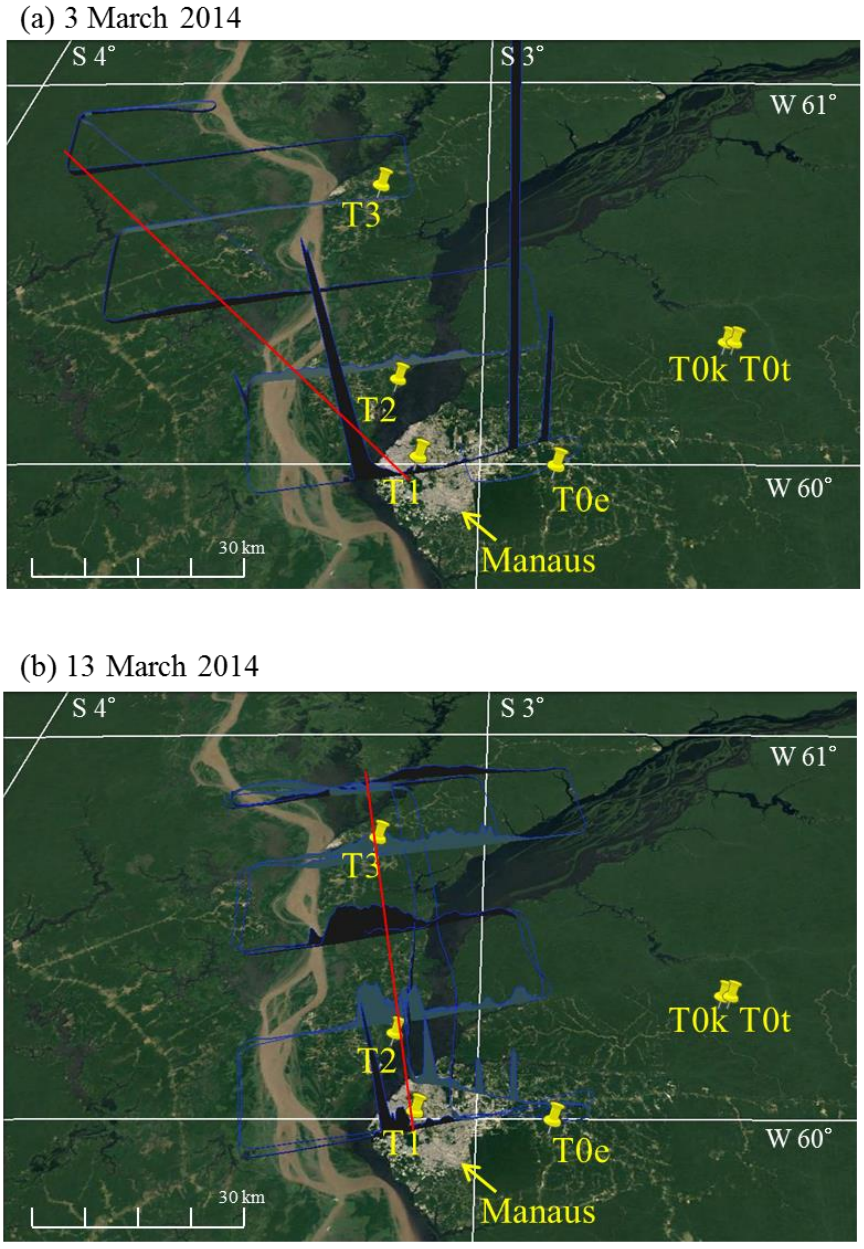

Figure S3. Visualization of the Manaus pollution plume for (a) March 3, 2014, 17:45 – 19:26 UTC, and (b) March 13, 2014, 14:14 – 17:21 UTC. The direction and extent of the plume observed within the boundary layer in the Manaus environs by the G-1 aircraft is represented by plotting NO_y concentrations on a vertical axis (0.13 to 369 ppb on March 3 and 0.10 to 75 ppb on March 13). The red lines guide the eye through the central axis of the plume. An image of land cover is in the horizontal plane. Yellow pins indicate the locations of some of the GoAmazon2014/5 research sites, including T3 (Martin et al., 2016).

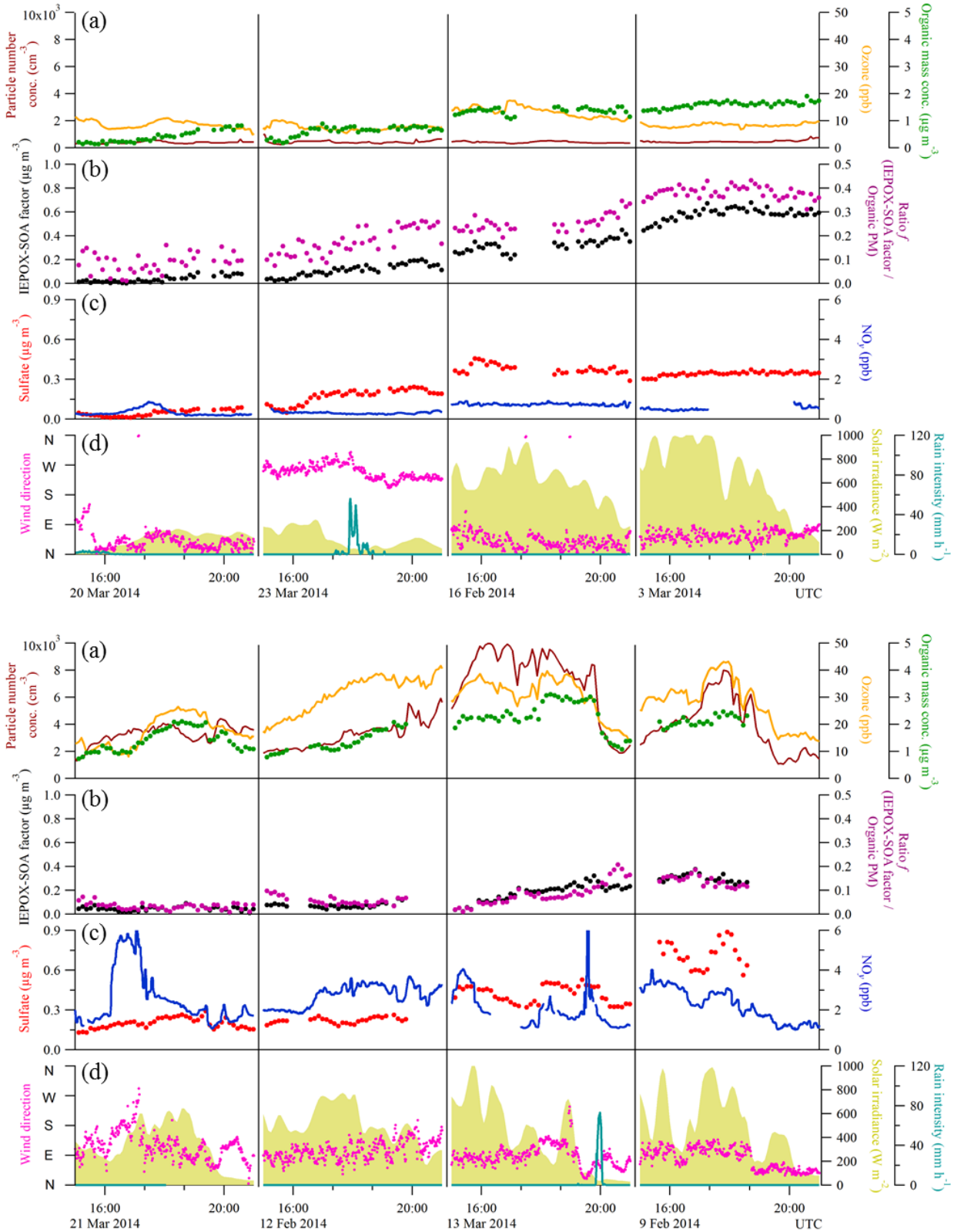

Figure S4. Selected cases of data sets collected during background and polluted conditions (top and bottom panels, respectively) as observed during afternoons at the T3 site.

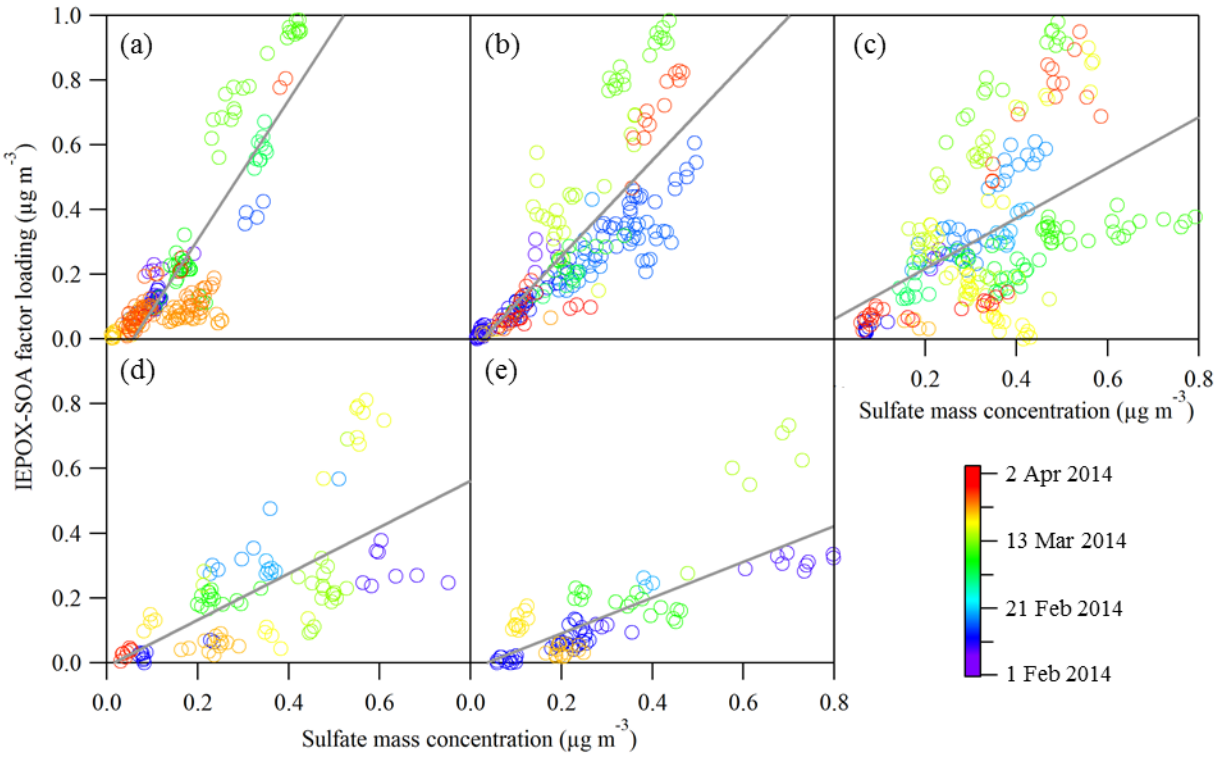

Figure S5. Scatter plots of sulfate mass concentration and IEPOX-SOA factor loading for local afternoon (12:00-16:00 local time; 16:00-20:00 UTC) for five different ranges of NO_y concentrations. Panels a-e correspond to groups labeled 1-5 according to Table 1. Table 1 presents the parameters of the six least-squares linear fits represented by the lines in the figure. Data is colored by date.

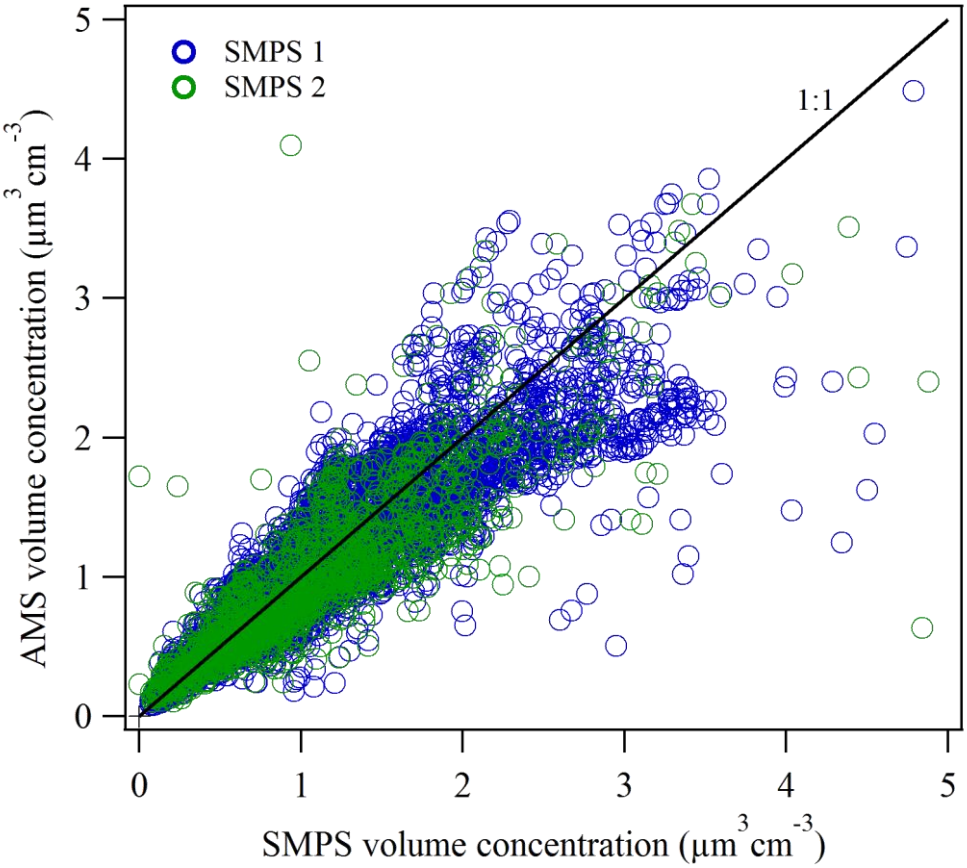

Figure S6. Scatter plot of AMS PM volume concentrations and SMPS PM volume concentrations. SMPS1 measured particles having mobility diameters of 10 to 461 nm from February 7 to March 28, 2014. SMPS2 measured particles having mobility diameters of 10 to 510 nm from February 24 to March 30. Material densities used in the calculation of AMS volume from AMS mass were based on a mixing rule for the five AMS-measured species. The material density of the organic component was calculated following the method of Kuwata et al. (2011) based on O:C and H:C values, which in turn were calculated following the method of Canagaratna et al. (2015).

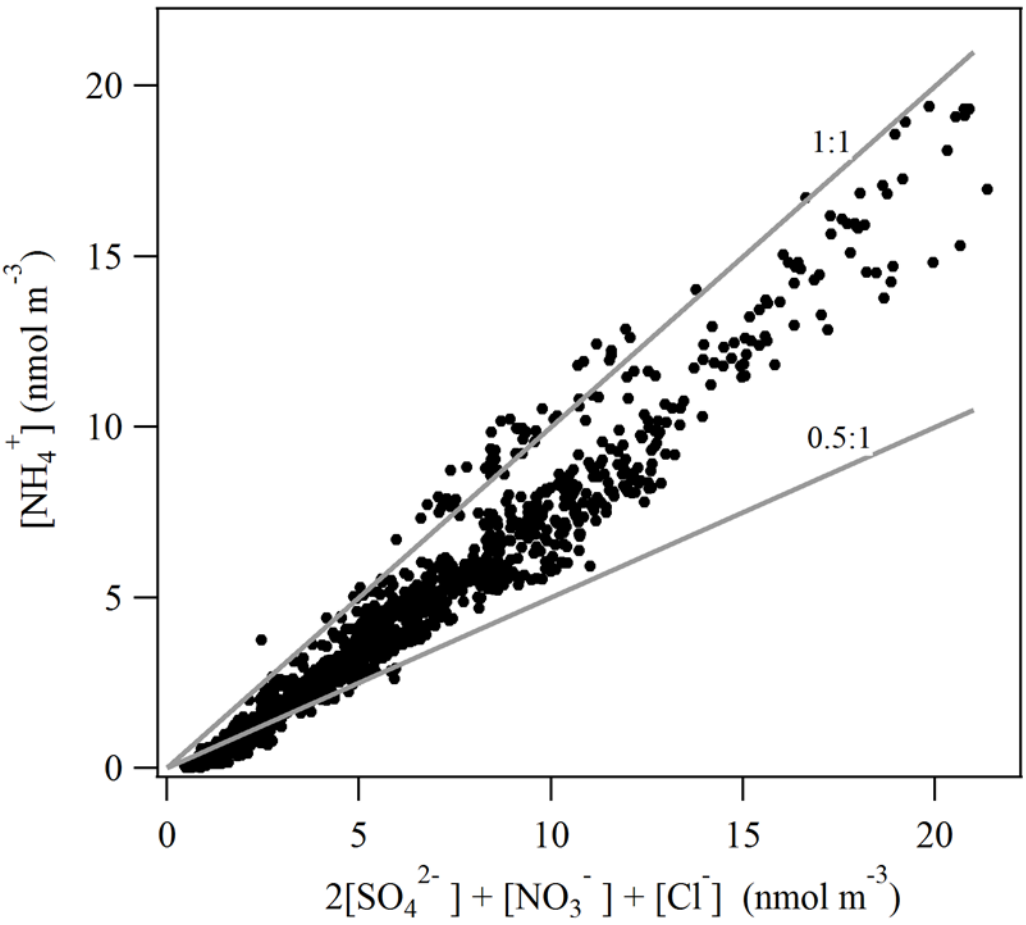

Figure S7. Ion balance for AMS measured species. A scatter plot is shown of mass concentrations of cations on the ordinate and of anions on the abscissa. Solid gray lines indicate relationships of 1:1 and 0.5:1.

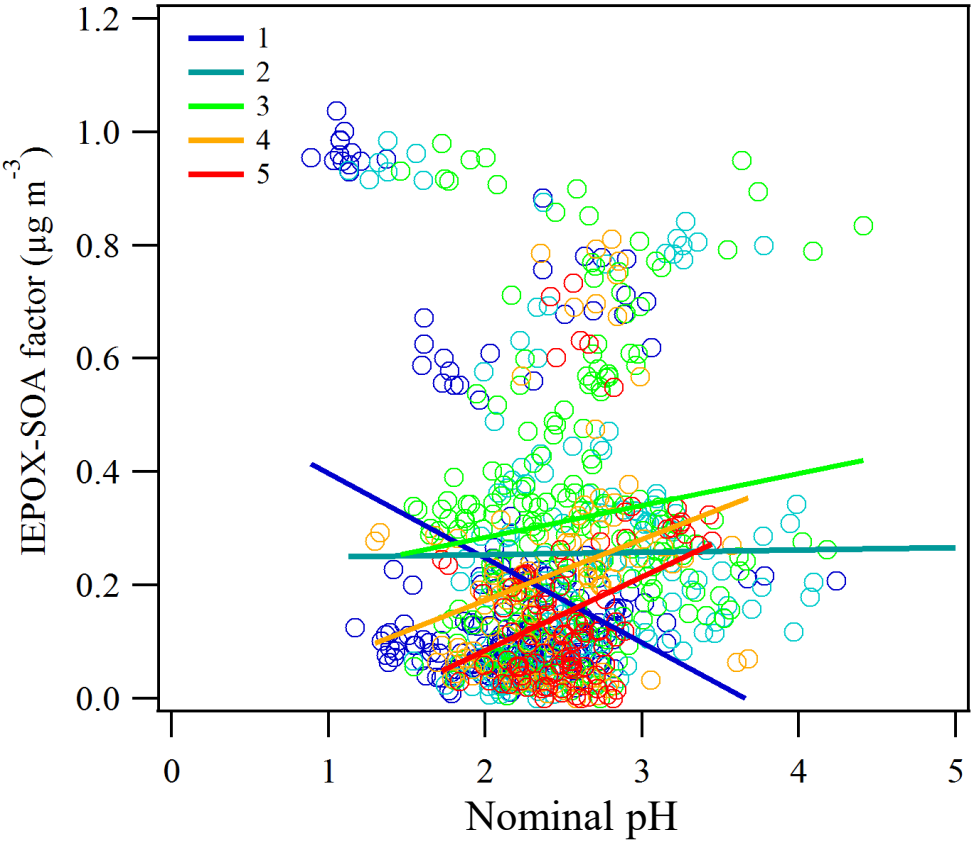

Figure S8. Scatter plot of estimated pH and IEPOX-SOA factor loading for local afternoon (12:00-16:00 local time; 16:00-20:00 UTC). The data sets were collected into five subsets, colored and labeled 1 to 5, based on NO_y concentration (analogous to analysis shown in Figure 6a).

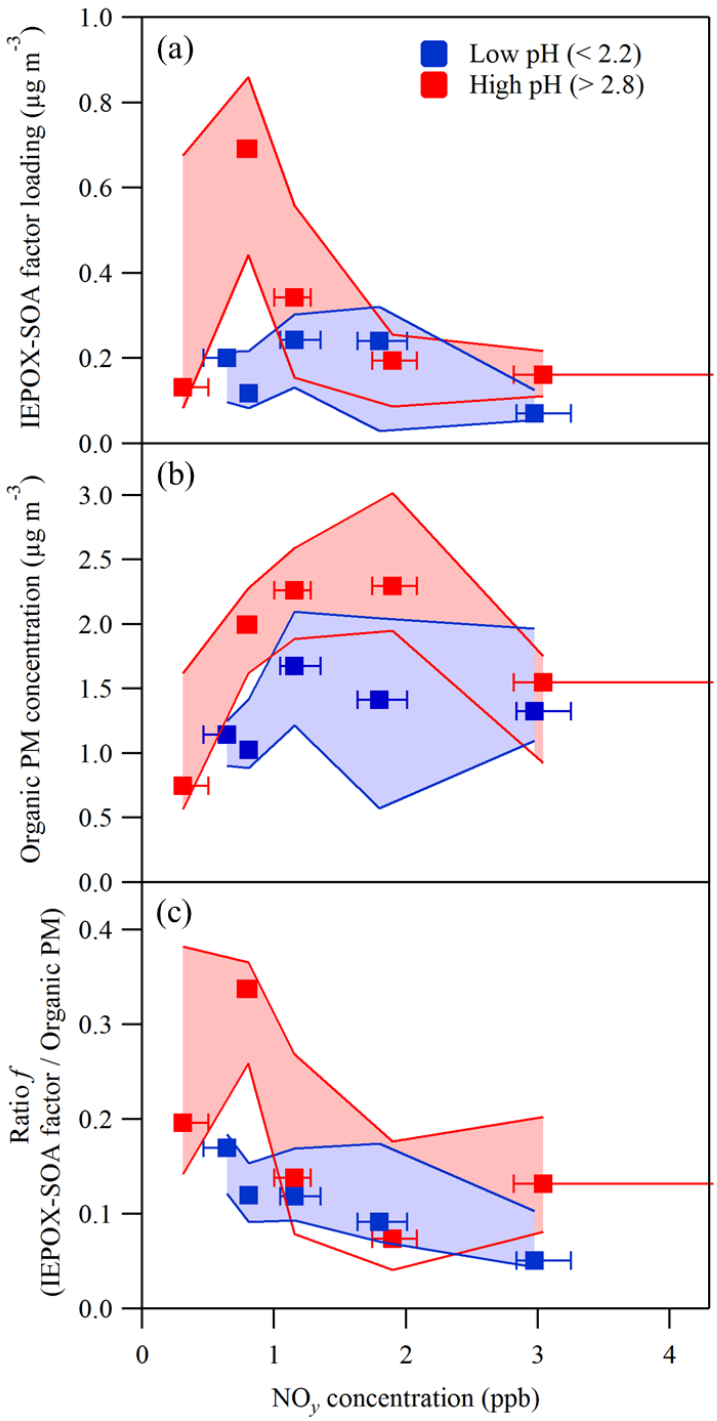

Figure S9. Dependence on NO_y concentration of (a) IEPOX-SOA factor loading, (b) organic mass concentration, and (c) the ratio *f* of the IEPOX-SOA factor loading to the organic PM concentration. Data are segregated by low (< 2.2) and high (> 2.8) pH and grouped into five levels of NO_y concentration (Figure 7). Squares represent medians of each group. Interquartile ranges are represented by whiskers along the abscissa and shading along the ordinate. The plotted data sets were recorded during local afternoon (12:00-16:00 local time; 16:00-20:00 UTC).